WAVE FORCES ON

LARGE SUBMERGED TANKS

Prepared by

C. J. GARRISON and R. H. SNIDER

Coastal and Ocean Engineering Division
Texas Engineering Experiment Station

Sea Grant Publication No. 210

COE Report No. 117

WAVE FORCES ON LARGE SUBMERGED TANKS

by

C. J. Garrison and R. H. Snider
Coastal and Ocean Engineering Division
Texas A&M University

January 1970

ABSTRACT

Wave induced forces acting on a hemispherical tank located
on the ocean floor are studied both experimentally and theoretically.
The effect of the wave height, wave length, water depth and size
of the tank is investigated for the case of a hemispherical tank.
The results of the investigation include horizontal and vertical
forces as well as pressure measurements on the surface of the hemi-
sphere presented in dimensionless form as a function of wave number,
relative water depth and relative wave height. The results obtained
have direct application in the design of large submerged structures
such as oil storage tanks.

PREFACE

This report was primarily written by R. H. Snider in partial fulfillment of the Master of Science degree under the supervision of Dr. C. J. Garrison. This report is part of a more comprehensive study on wave forces on large submerged ellipsoidal tanks being directed by Dr. Garrison.

TABLE OF CONTENTS

LIST OF FIGURES

CHAPTER I

INTRODUCTION

In recent years ever increasing attention has been
given to construction and recovery of petroleum in the
coastal waters of the oceans. In the design of large off-
shore structures such as large submerged oil storage tanks
it is necessary to have an understanding of the forces
induced by such phenomena as gravity waves. In the pre-
sent study an experimental approach to the problem of wave
interaction with large hemispherical tanks is taken. Al-
though the shape considered is somewhat idealized it is
representative of practical shapes and the results provide
much of the insight needed to understand the interaction
with more complex geometries.

One new concept in offshore oil production for ex-
ample involves the use of very large submerged oil storage
tanks. The Chicago Bridge and Iron Company has constructed
a 500,000 barrel underwater oil storage tank which is 270
feet in diameter and 205 feet high. In the design of
these large tanks existing knowledge regarding the wave
force associated with such structures as piles does not
apply. The present study was directed at understanding

"The citations on the following pages follow the style
of the _Journal_ _of_ _the_ _Hydraulics_ _Division_, Proceedings of
the American Society of Civil Engineers."

the forces on these large objects by use of a simplified theory and testing. The results of the present study provide wave forces (horizontal and up-lift) as well as the instantaneous pressure distribution acting on the surface of the object.

Review of Literature

The force exerted on vertical circular cylinders or piles by ocean waves has been the subject of intensive investigation for nearly the past twenty years. Essentially all of these studies were based on the well-known "Morison equation" (7) which involves both a drag and inertia component of force. Moreover, in the case of small objects such as piles, the wave length in most practical cases is large compared to the pile diameter and the "Morison equation" is valid as a basis for analysis. This Morison approach does not apply to large structures such as submerged tanks because of the relative size of the structure and wave length and the effect of the free surface.

The horizontal and vertical components of force acting on a submerged sphere that is small compared with the wave length and water depth have been studied by O'Brien and Morison (8). From their laboratory investigations, they obtained one set of data by measuring the time history

of the horizontal component of force on a sphere suspended
at different distances below the water surface. By mea-
suring the horizontal force record at the wave crest,
trough, and when the two still water levels passed the
center of the sphere, values of drag and inertial force
were computed. Another set of data was obtained by set-
ting a sphere on a razor edge tee at the bottom of the
wave channel, holding the wave period constant, and vary-
ing the wave height very slowly until the sphere just
moved off the tee. The up-lift force at this instant was
considered to be the maximum vertical force and to be
equal to the weight of the sphere in water.

The magnitude and characteristics of forces resulting
from oscillatory waves were determined for models of sub-
merged barge-line structures by Brater, McNown, and Stair
(2). The wave profiles and the variation with the time
of the resulting horizontal and vertical forces were ob-
tained for various wave heights, wave periods, and loca-
tions of the barge with respect to the water surface (no
measurements were made with the barge on the bottom).
The basic model was a right parallelepiped having propor-
tions of a typical barge. These investigators in their
studies of various barge configurations neglected the
convective acceleration terms of force due to drag, since
the inertial forces predominated owing to the size of the

structures relative to the wave height. They chose to use the equations for pressure at the upward and downwave ends of the barges which were mounted normal to the direction of wave advance. These studies provided design data needed for the application of analytical methods in the determination of forces on some types of submerged structures.

Harleman and Shapiro (5) have treated the case of the forced oscillations of moored and fixed spheres beneath a train of waves. Their theoretical development of a differential equation describing the motion of the object includes a nonlinear term due to square-law damping. By replacing the nonlinear damping term by an equivalent linear damping term, the equation is rendered solvable. The solution occurs in the form of ratios of the forces and displacements for the moored case to forces and geometrical parameters for the rigidly fixed case. This approach is applicable for any submerged object for which the wave force can be predicted for the case of a rigidly fixed object.

Grace and Casciano (4) have conducted a program of ocean testing of the wave-induced forces on a bottom-mounted sphere. In their work, concurrent records of wave pressure and force on a sphere mounted near the sea floor in 25 feet of water were obtained. Surface wave

characteristics, and the resulting particle kinematics, were calculated from the pressure record using Stoke's third-order theory, and the computed particle velocities and accelerations for individual waves were then combined with the measured forces to obtain force coefficients. Their program of ocean testing a submerged sphere provides a probabilistic method of choosing force coefficients to evaluate the maximum total force on subsurface objects such as small storage tanks and diver habitats.

In the case of large submerged objects such as large submerged oil storage tanks the wave length is not always large relative to the dimensions of the object and the simplification that comes about due to the relative size of the structure and design wave is not possible. The incident wave is scattered upon encountering a large object and, therefore, the assumption that the object does not affect the incident wave is no longer valid. Thus, a different and more basic approach to the problem than that used by some of the previously mentioned investigators is required.

Although the condition of finite ratio of object size to wave length tends to complicate the problem, the fact that the object is large compared to the wave height in most practical cases of large tanks tends to simplify things somewhat. The excursion dimensions of the fluid

particles under a wave are proportional to the wave height
and, therefore, the ratio of wave height to object size
is an important parameter with regard to viscous effects.
If this parameter is small, which is the case of practi-
cal interest, the amplitude of the fluid motion is small
compared to the object size and, as has been shown by
Sarpkaya and Garrison (9), viscous effects are unimportant
since the fluid must travel a distance of the order of
half a diameter before the trailing vortices develop and
separation sets in. Thus, disregarding viscous effects,
a potential flow analysis is appropriate and viscous drag
may be ignored. It is on this basis that a simplified
potential flow analysis is used although it is well-known
that upon increasing the wave height, a point will be
reached where viscous effects will become important and
the theory will become invalid.

Experimental Objective

In order to obtain practical information on the in-
teraction of a large submerged oil storage tank with ocean
waves, this research was focused on the measurement of
wave induced forces acting on a hemispherical object lo-
cated on the ocean floor. A second goal was to present
a comparison of both experimental and theoretical effects
of wave height, wave length, water depth, and object size

on the submerged hemisphere.

The results of this study include direct measurements of horizontal and vertical forces as well as forces calculated by integrating the complete instantaneous pressure distribution over the surface of the submerged hemisphere. These results, presented in dimensionless form as a function of the wave number, relative water depth, and relative wave height, have a direct application in the design of large submerged structures such as oil storage tanks.

The work reported in this thesis is a part of a larger program on wave forces on submerged objects being carried out at Texas A&M University under the direction of Dr. Garrison. The overall program involves the theoretical analysis of a submerged ellipsoid which is valid for all values of the ratio of tank size to wave length. The final goal of this program will be the theoretical treatment for arbitrary shape tanks as well as experimental verification.

CHAPTER II

EXPERIMENTAL EQUIPMENT

Two-Dimensional Wind-Wave Channel

The work for this experimental investigation was conducted in the two-dimensional wind-wave channel (See Figure 1) in the Hydromechanics Laboratories of Texas A&M University. The 120 feet long, 3 feet deep and 2 feet wide wave channel has a steel-plated bottom welded to large supporting wide flange beams. Heavy duty 3/8 inch thick glass wall panels, held in place by steel angles and metal stripping, allow for maximum visual observation. The tank is equipped with a paddle-type wave generator capable of producing 2.5 feet to 25 feet wave lengths at heights up to 11 inches. At the far end of the tank is a perforated beach type wave absorber. A wave filter con-structed of wire mesh was installed in the wave channel near the generator end for purposes of eliminating the short wave length components. The speed of the wave pad-dle was electrically controlled with its eccentricity operated manually.

Hemispherical Models--Wave Force and
Pressure Distribution Models

The need for two identical hemispherical models was
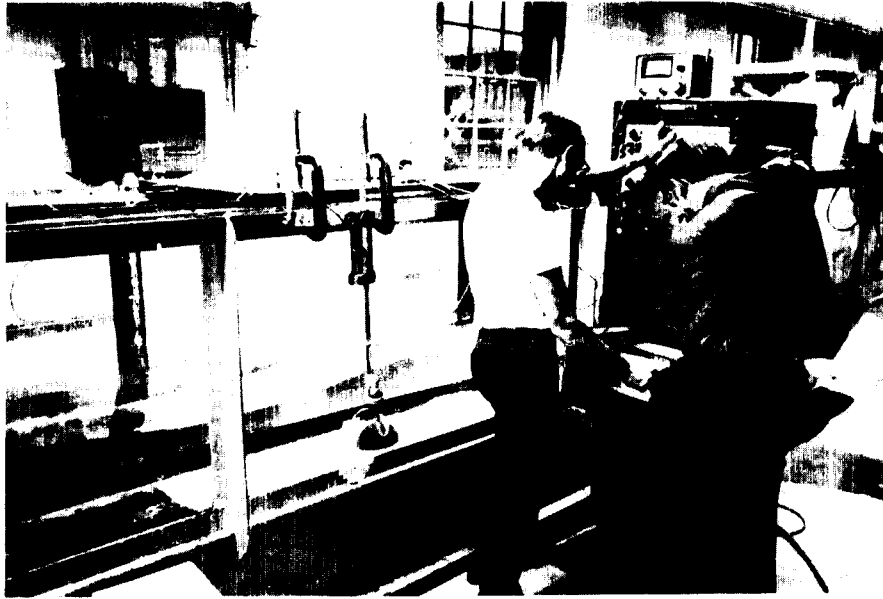
Figure 1. Two-dimensional wind-wave channel and experimental equipment.
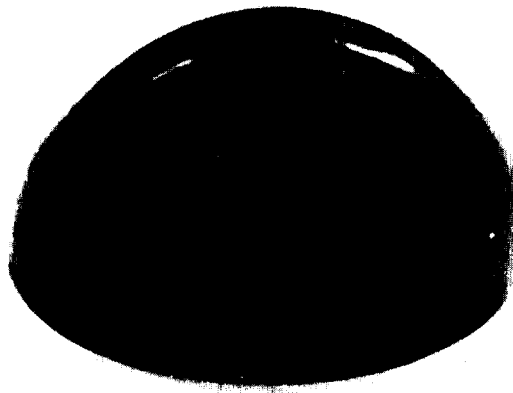
Figure 2. Hemispherical model.

met inexpensively by utilizing a plastic toy ball. When bisected, the ball provided two 7 inch diameter by 1/16 inch thich hemispherical shells (See Figure 2).

The hemispherical wave force model (See Figure 3) was basically constructed of two components; the shell and a ½ inch thick plexiglas stiffening ring. The plexiglas stiffener was inserted ½ inches into the model to allow for a 3/4 pound, 5 inch diameter by 1/8 inch thick, steel ring which was used for ballast weight. The recessing of the plexiglas ring from the edge of the shell also eliminated the possibility of flow passing underneath the model affecting the force. The configuration of both the stiffener and ballast weight permitted the model to fill freely with water. Also, a 1/32 inch air hole at the top of the model eliminated the chance of air bubbles forming while the shell filled.

The wave force model was suspended by a three point system on 0.008 inch steel wire with its horizontal movement restrained by two 0.008 inch wires (See Figure 4). The vertical support wires were passed directly through the model and plexiglas stiffener to 1/8 inch eye bolts. The horizontal restraining wires were connected to the bottom of the shell by passing the wires underneath the model to the eye bolt fasteners. Two notches were scored on the skirt of the model to accurately guide the
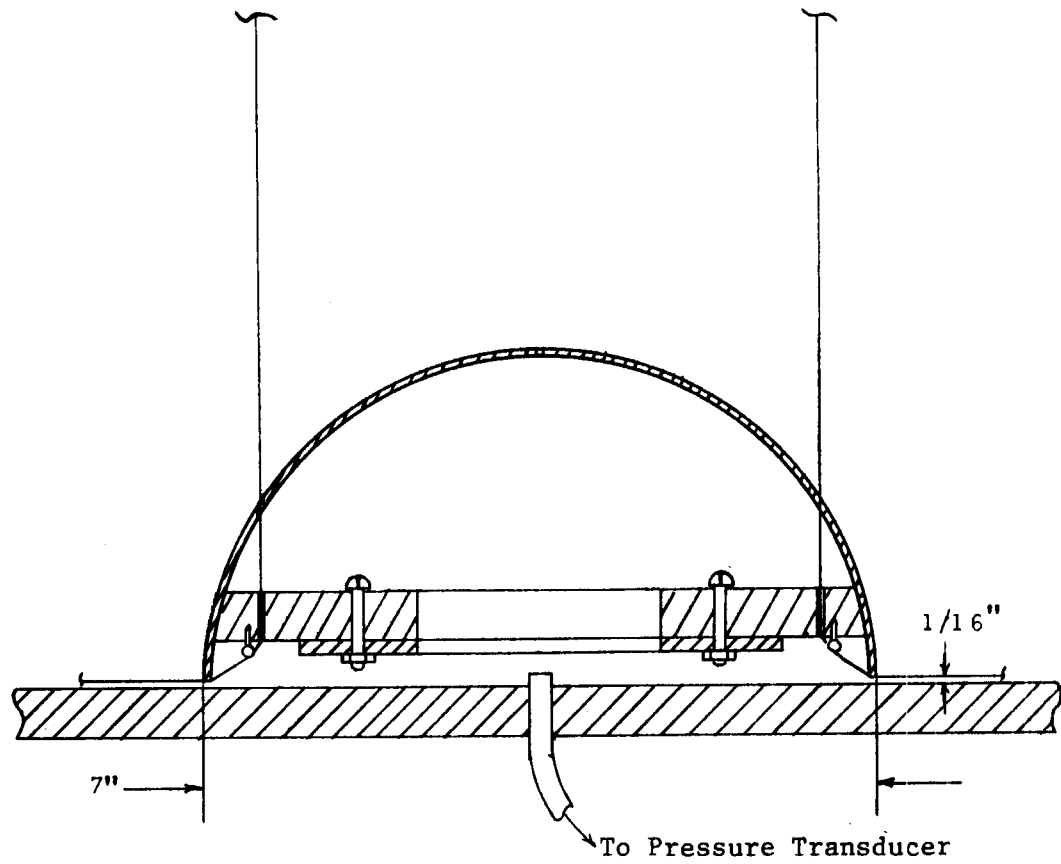
Figure 3. Hemispherical wave force model and pressure tap.

Horizontal Load Cells

Vertical Load Cells

Plexiglas Pulleys
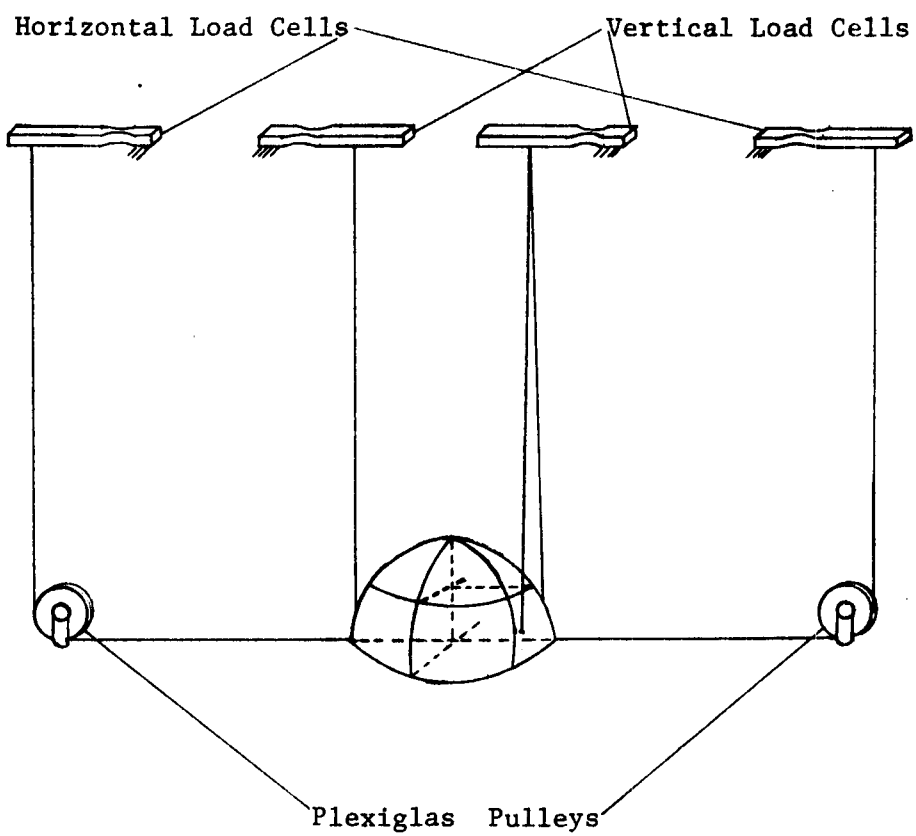
Figure 4.   Hemispherical wave force model.

horizontal wires out from underneath the model and along the tank's horizontal axis.

In order to measure the pressure fluctuation inside the model due to the 1/16 inch clearance between the shell and the channel floor (See Figure 3), a ¼ inch pressure tap was drilled underneath the model through the wave channel floor. The pressure tap was connected to a length of ¼ inch flexible copper tubing running from the channel floor to a pressure transducer located outside the wave channel. Except for short flexible lengths on either end, copper tubing was used as opposed to a flexible plastic or rubber tubing so that the frequency response of the system would be as large as possible.

For visual contrast the shell was sanded and painted with an orange industrial enamel. The wave channel floor was painted with three coats of red yacht anti-fouling bottom paint and three subsequent coats of rust-resistant high gloss white marine enamel. To give the coatings a smooth finish the surface was polished with 400 grit emery cloth. The orange of the model and the smooth white finish of the wave channel floor provided the proper contrast for the hemisphere to be visually adjusted to within the 1/16 inch clearance above the floor.

A second model, identical in shape to the first one, was specially designed and constructed for purposes of

measuring the instantaneous pressure distribution. This model was weighted to set firmly on the floor of the wave channel and was held on center by a disc which fit inside the edge of the shell and allowed it to be rotated (See Figure 5).

A series of 5 piezometer taps were drilled along a meridional line of the model at 18 degree intervals starting at 9 degrees from horizontal and ending 9 degrees from vertical. A short flexible length of tubing was attached to the ¼ inch copper tubing which was connected to the pressure transducer and extended through the wave channel floor so that each piezometer tap could be connected individually. By connecting the flexible length to each of the piezometer taps and rotating the model through 180 degrees at 18 degree intervals the pressure on the surface of the hemisphere could be read at 55 different points on half of the hemisphere.

The construction of the pressure distribution model was similar to the force model in that it consisted of a 1/16 inch thick shell stiffened with plexiglas rings cemented on the inside. One stiffening rib was placed behind the piezometer taps. The piezometer taps were connected by ¼ inch holes drilled in this rib which provided a snug fit with the flexible line.

To provide azimuth settings during the test, lines

Piezometer Openings

18°

18°

18°

18°

18°

9°

3/32"

7"

To Pressure Transducer
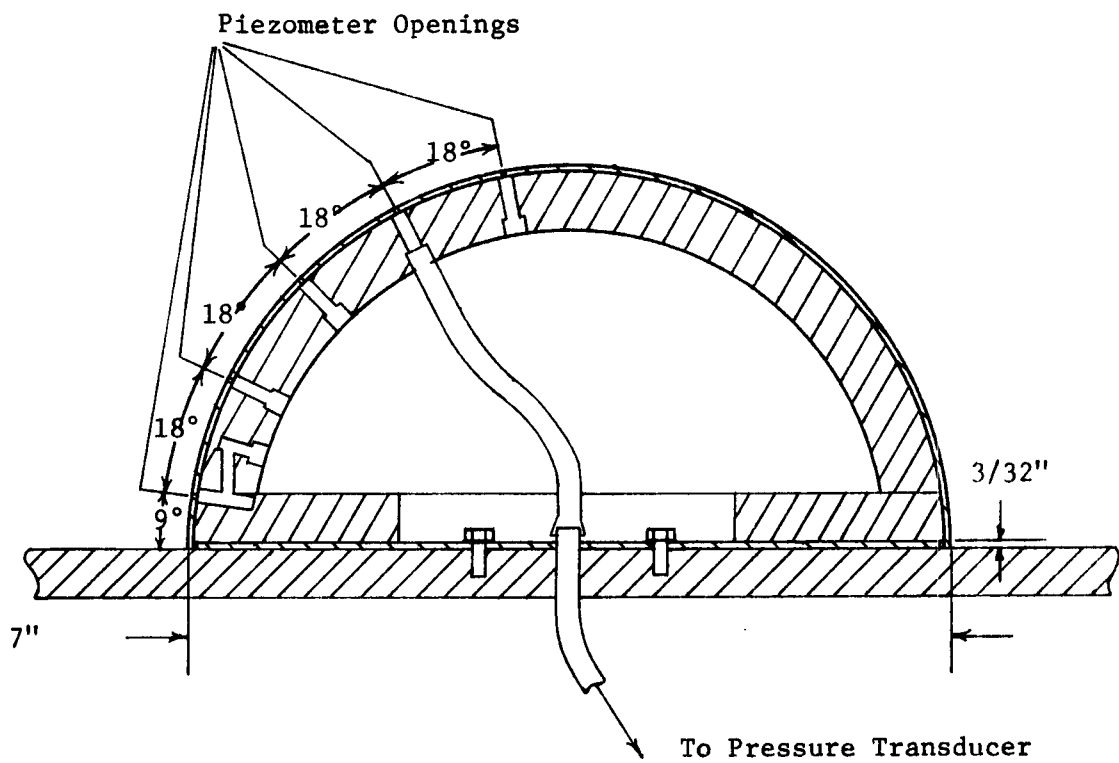
Figure 5. Hemispherical pressure distribution model and pressure
tap.

were drawn radially from the center of the aluminum disc
on the white surface of the wave channel floor. These
lines were drawn at 18 degree intervals starting from the
upstream axis moving counterclockwise through 180 degrees.
The pressure was then recorded at 55 points on the sur-
face of the hemisphere by connecting the flexible tygon
tube to one of the pressure taps and reading the pressure
at each of the eleven azimuth settings.

Horizontal and Vertical Force Load Cell System

In order to measure the horizontal and vertical wave
forces, the model was suspended by fine wires from strain
gage load cells (See Figure 6). Three vertical wires at-
tached to strain gaged beams were used to support the
model in the vertical direction. Adjustments screws were
provided at the top ends for the purpose of adjusting the
model to a clearance of approximately 1/16 inch above the
wave channel floor.

To restrain the model in the horizontal direction
and also to measure the horizontal component of force,
the model was held by two pretensioned fine wires which
were passed around pulleys and connected to two strain
gaged beam load cells (See Figure 4). The pulleys were
specially made of plexiglas with small ball bearings at
the centers. The combined effect of its large diameter
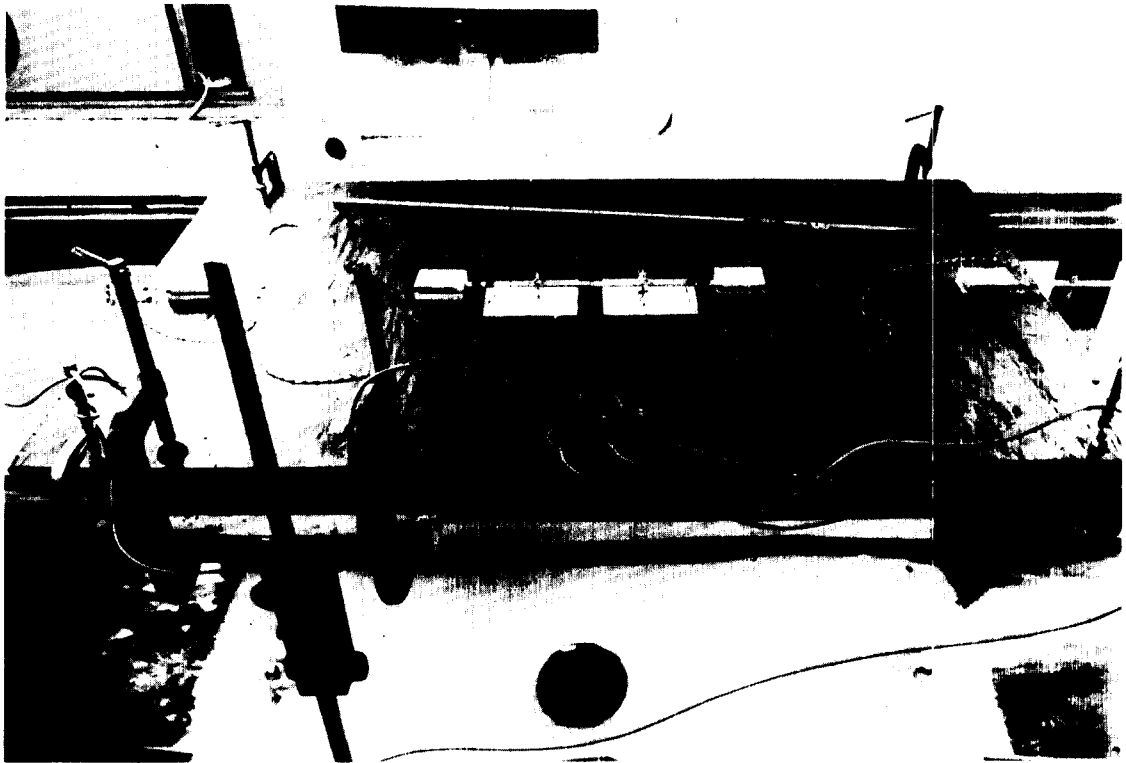
Figure 6.   Beam/strain gage load cell system.

(5 inches) and ball bearings reduced the errors introduced in the force readings due to friction effects of the pulleys.

The supporting wires were all attached to load cells which were mounted on a board laid across the wave channel. The load cells consisted of a cantilever beam with strain gages mounted at a necked down section near the support. Two strain gages were mounted on each beam so that one operated in tension and one in compression. These gages were connected in a Wheatstone bridge in such a way that the individual forces were additive.

The beams were made of 3/32 inch aluminum stock, ½ inch wide and 8 inches long. The beams were necked down to ¼ inch width at the place where the strain gages were attached. The moment arm (wire attachment point to strain gage distance) was 3 inches.

Two beams were used to measure the horizontal force. The wires connecting the two beams were pretensioned so that they never became slack and the strain gages were connected so that their outputs were additive. The wiring diagram for the horizontal paired strain gages are shown in Figure (7).

Two beams were also used to measure the vertical force. Since the model was suspended vertically by three wires one beam supported one wire while the other beam
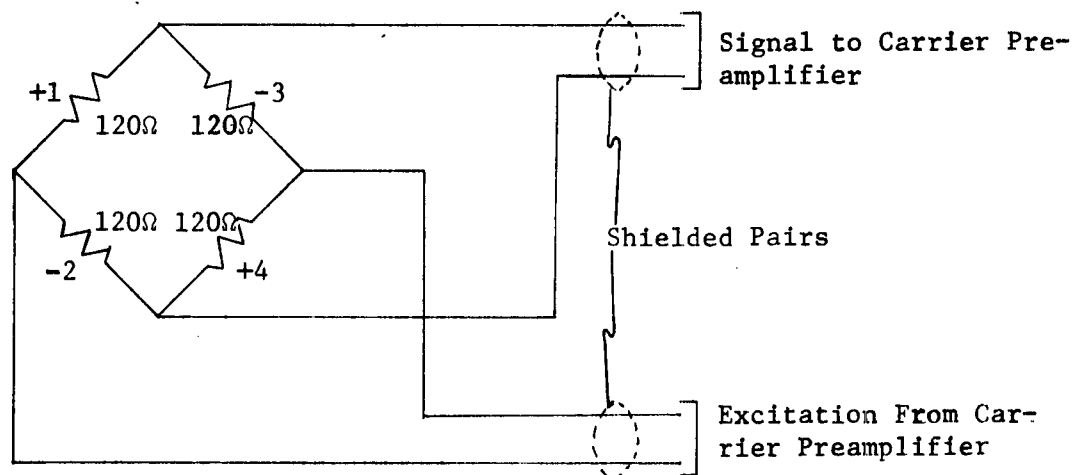
Figure 7. Full-bridge connections to measure horizontal force output.
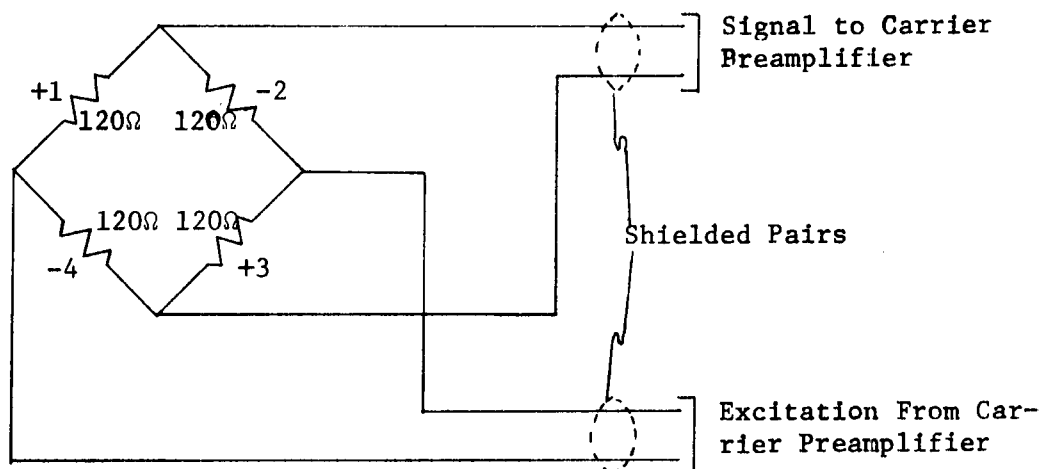
Figure 8. Full-bridge connections to measure vertical force output.

equipped with a cross bar supported two wires. These strain gages were also connected so that the signals were additive. The wiring diagram for the vertical force beams is shown in Figure (8).

Two channels of a four channel Sanborn 150 carrier amplifier/recorder were used to record both the horizontal and vertical forces.

Resistance Wave Height Gage

A parallel wire resistance type wave gage was used for this experimental investigation because of its response to small magnitudes of wave height. This type of gage operates on the principle that the conductance between the two parallel submerged wires varies proportionally to the length of wire submerged.

The wave gage was wired parallel to one leg of a Wheatstone bridge as depicted in Figure (9). Since the wave gage resistance could not be offset by the internal resistance of the carrier amplifier an external variable wire wound resistor was connected across an opposite leg of the bridge for purposes of balancing the bridge. This circuit was used in conjunction with a carrier amplifier and read out on one channel of a four channel 150 Sanborn amplifier/recorder.

The wave height gage as shown in Figure (10) consisted
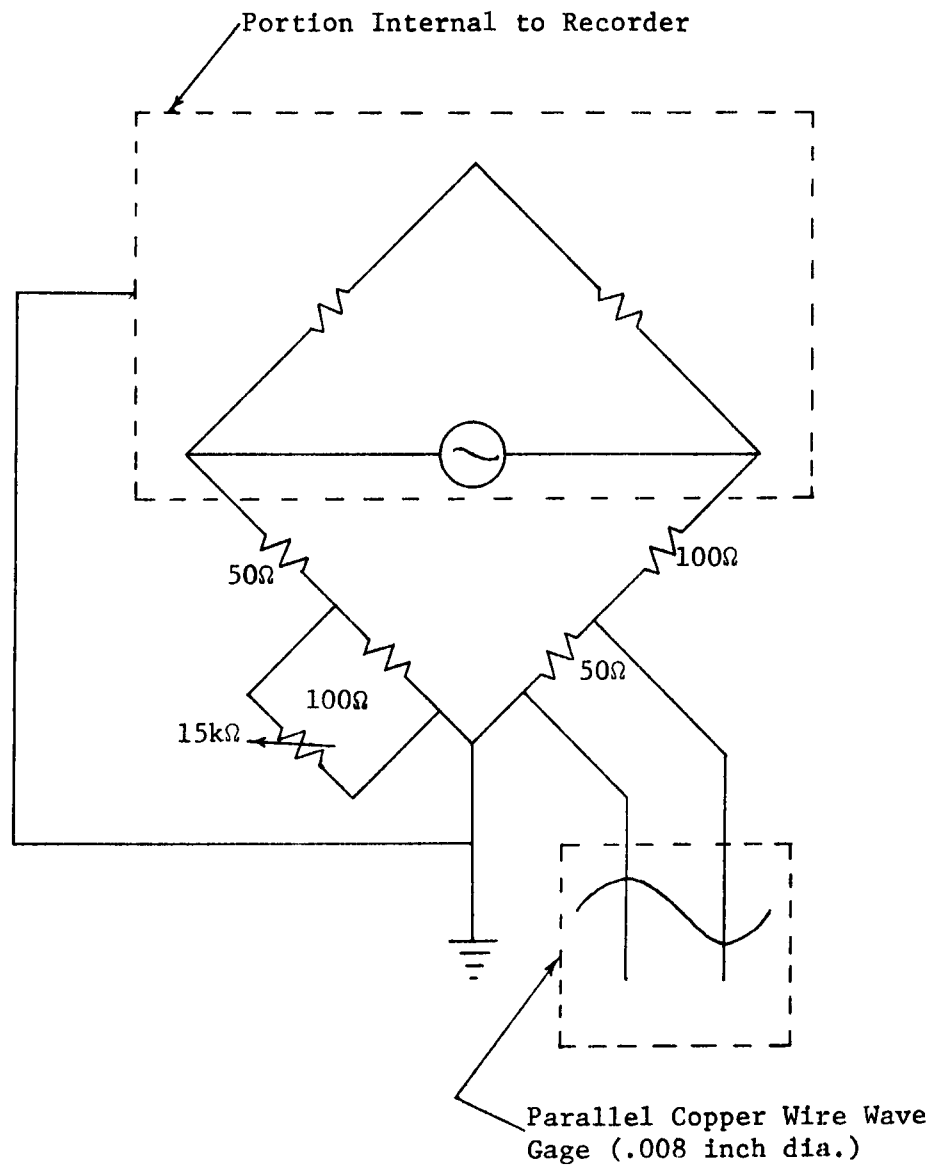
Figure 9. Half-bridge connections for resistance wave gage.

Figure 10.   Resistance wave height gage.

of a light frame which held two parallel copper wires .008 inches in diameter spaced ¼ inch apart. The wires were held by plexiglas insulators which were mounted on the frame.

The wave gage was mounted on a Leupold and Stevens point gage and calibration was carried out by adjusting the submergence of the wires by use of the point gage.

Pressure Transducer

The wave force model was suspended with a small clearance above the channel floor so that no force would transmit through any path other than that of the load cells. As a result of this clearance the pressure inside the hemisphere was not constant but fluctuated and therefore contributed to the measured vertical force. Thus, it was necessary to locate a pressure tap (connected to the pressure transducer) inside the hemisphere to measure the pressure so that the vertical force could be corrected by the amount of the interior pressure contribution.

After the force measurements were obtained from the wave force model tests, a second hemispherical model was provided to measure the instantaneous pressure distribution on its surface. This model (pressure distribution model) has a series of piezometer taps located along a meridional line on its surface. To measure the pressure

at each piezometer tap a Pace pressure transducer (located on the outside of the wave channel) was connected to a copper tubing pressure tap leading to the inside of the hemisphere. From the pressure tap inside the model a tygon tube, long enough to reach any of the piezometer taps, was connected to one of the piezometer taps and the pressure was recorded at various azimuth settings. In this way the complete pressure distribution over the surface of the model was obtained.

The pressure transducer was operated in conjunction with a Pace Model CD25 Transducer Indicator and the indicator output was read out on one channel of a four-channel Sanborn 150 amplifier/recorder.

The pressure transducer was mounted on a Leupold and Stevens point gage at approximately the free surface elevation and calibration was carried out by adjusting the transducer through positive and negative pressure head readings by use of the point gage.

Experimental Procedure

The experimental procedures for both the wave force and pressure distribution test models were basically similar.

Before each test run a careful preparation of the experimental equipment was made. This involved filling

the wave channel to the desired depth; balancing the pre-amplifying equipment; calibrating the gaging systems; and selecting the proper attenuation for each preamplifier.

To provide a check of the calibrations for the wave force and pressure distribution model tests, both initial and final calibrations were taken for each test run.

Both the wave height gage and the pressure transducer were mounted on Leupold and Stevens point gages. The calibration of the wave gage was carried out by adjusting the submergence of its parallel wires by moving the point gage through increments of 0.02 feet. The calibration of the pressure transducer was achieved by adjusting the transducer through positive and negative pressure head readings (increments of 0.02 feet) by use of the point gage.

To calibrate the horizontal load cells, three 50 gram weights were hung from each gaging beam in 50 gram increments up to 150 grams of total calibration weight.

To calibrate the vertical load cells, four 10 gram weights were centered on top of the wave force model in 10 gram increments up to 40 grams total weight.

Preparations for individual runs varied in time according to various difficulties encounted, with the time for each test run taking approximately two hours.

CHAPTER III

THEORETICAL CONSIDERATIONS

In the following a theory developed by Dr. C. J.
Garrison (3) is presented for wave forces on submerged
hemispherical objects. The theory is based on two assump-
tions: (a) the wave length is large compared to the object
size and, (b) viscous effects are negligible.

In the case of large submerged objects such as large
submerged oil storage tanks the wave length is not always
large relative to the dimensions of the object and the
simplification that comes about due to assumption (a) is
not always possible. The incident wave is scattered upon
encountering a large object and, therefore, the assump-
tion that the object does not affect the incident wave is
not valid. Thus, a different and more basic approach to
the problem is needed. However, there are many cases
where assumption (a) is met and, therefore, a theory based
thereon is of considerable value.

Although the condition of finite ratio of object size
to wave length tends to complicate the problem of wave
interaction with large subsurface objects, the fact that
the object is large compared to the wave height in most
practical cases of large tanks tends to somewhat simplify
the matter. The excursion dimensions of the fluid parti-
cles under a wave are proportional to the wave height and,

therefore, the ratio of wave height to object size is an important parameter with regard to viscous effects. If this parameter is small, which is the case of practical interest as indicated in assumption (b), the amplitude of the fluid motion is small compared to the object size, and viscous effects are unimportant since the fluid must travel a distance of the order of half a diameter before the trailing vortices develop and separation sets in. Thus, in the following theoretical development a potential flow analysis for horizontal and vertical force is presented where viscous effects are disregarded. It is on this basis that a simplified potential flow analysis is used although it is well known that upon increasing the wave height, a point will be reached where viscous effects will become important and the theory will become invalid.

Progressive Linear Wave Theory

This section develops only the wave theory necessary to logically show the steps taken in formulating the equations which predict horizontal and vertical wave forces. For a detailed mathematical summary of wave theory see the text by Lamb (6).

The velocity potential (φ) of a gravity wave is given by

$$\varphi = \frac{Ag}{\sigma} \frac{\cosh k\ (h+Z)}{\cosh k\ h} \cos (kX - \sigma t) \qquad (3.1)$$

and the horizontal component of water particle velocity (u) by

$$u = -\frac{\partial \varphi}{\partial X} = -\left[-\frac{Agk}{\sigma} \frac{\cosh k(h+Z)}{\cosh k h} \sin (kX-\sigma t) \right] \quad (3.2)$$

The horizontal component of water particle "local" acceleration ($\dot{u}$) is

$$\dot{u} = \frac{\partial u}{\partial t} = - Agk \frac{\cosh k(h+Z)}{\cosh k h} \cos (kX-\sigma t) \quad (3.3)$$

The subsurface pressure (P) is

$$P = \rho gA \frac{\cosh k(h+Z)}{\cosh k h} \sin (kX-\sigma t) \quad (3.4)$$

The pressure gradient $\left(\frac{\partial P}{\partial X}\right)$ evaluated at the center of the hemisphere, i.e., X = o, Z = - h is

$$\frac{\partial P}{\partial X} = \frac{\rho gAk}{\cosh k h} \quad (3.5)$$

The horizontal dynamic buoyant force (F_B) is, therefore, given by

$$F_B = - \frac{\partial P}{\partial X} \forall = - \frac{\rho gAk \forall}{\cosh k h} \quad (3.6)$$

The horizontal force (F_I) due to the added mass effect of the object is

$$F_I = - \rho \forall C_m \frac{\partial u}{\partial t} \quad (3.7)$$

where $\frac{\partial u}{\partial t}$ is evaluated at X = o and Z = - h.

The combined or total horizontal force (F) is, then

$$F = F_I + F_B \tag{3.8}$$

and hence, the maximum total horizontal force (F_{Hmax}) is

$$F_{Hmax} = \frac{\rho \, \forall \, Agk(C_m+1)}{\cosh k \, h} \tag{3.9}$$

where the volume $(\forall)$ of the hemisphere is $\forall = 2/3 \, \pi \, a^3$.

It has been shown by Stokes (10) that when a solid body is in motion in a frictionless fluid of infinite extent, the effect of the fluid pressure is equivalent to an increase in the inertia of the body. In the case of a sphere, the magnitude of the increase of inertia has been analytically determined to be one-half of the mass of fluid displaced. The hemisphere represents the "mirrored image" of the sphere in a frictionless fluid of infinite extent; therefore, the induced mass coefficient (C_m) for the hemisphere is also one-half of the mass of fluid displaced.

Writing equation (3.9) in a dimensionless form and substituting $C_m = 0.5$, the following expression for horizontal force coefficient is obtained:

$$f_x = \frac{F_{Hmax}}{\gamma \, a^2 H/2} = \frac{\pi}{\cosh \frac{h}{a} \frac{2\pi a}{L}} \frac{2\pi a}{L} \tag{3.10}$$

Equation (3.10) is plotted in Figure (13) in the form of the force coefficient as a function of $2\pi a/L$ for various values of the water depth to tank height ratio.

These theoretical curves are compared in Chapter IV with measured horizontal force data taken from both the wave force and pressure distribution models.

The following development for the maximum vertical force on a hemispherical object, is based upon Krilov Hypothesis (1) where: "every point of the submerged surface of a ship experiences a hydrodynamic pressure such that its value is determined by the equation of the wave motion for the corresponding fluid point". From this hypothesis, the following expression for vertical force was obtained by integrating the pressure over the surface area of a hemisphere as indicated in Figure (11).
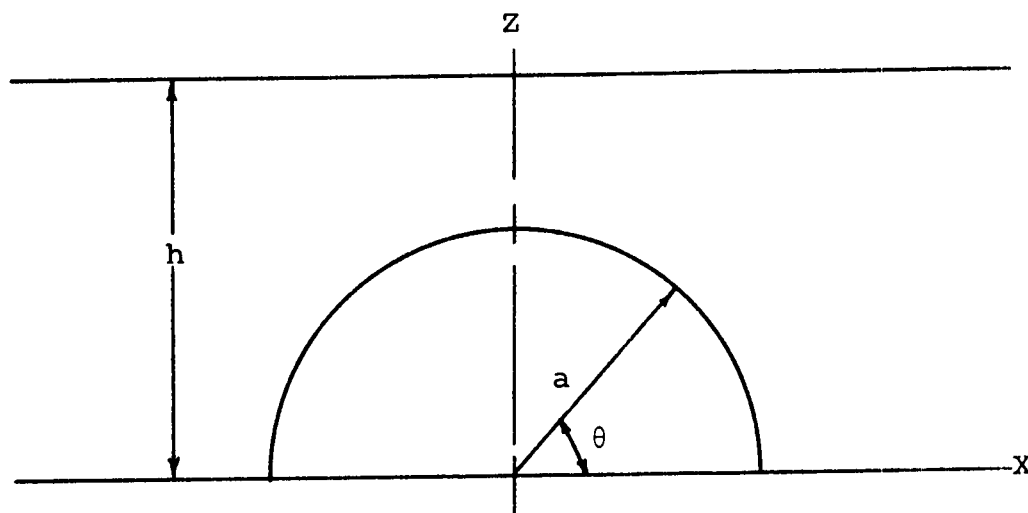
Figure 11. Cross-sectional view of hemispherical pressure distribution model.

The pressure (P) within the fluid is

$$P = \rho g \frac{H}{2} \frac{\cosh k(h+Z)}{\cosh k h} \cos (kX - \sigma t) \qquad (3.11)$$

and the hydrodynamic vertical force (F_V) is

$$F_V = \int P dA \sin \theta \qquad (3.12)$$

where $dA = 2\pi a \cos \theta \; a d \theta = 2\pi a^2 \cos \theta \; d \theta$

The maximum hydrodynamic vertical force (F_{Vmax}) is, then

$$F_{Vmax} = \int_{0}^{\frac{\pi}{2}} = 2\pi a^2 \sin \theta \cos \theta \; P d \theta$$

or, substituting for pressure yields

$$F_{Vmax} = \int_{0}^{\frac{\pi}{2}} 2\pi a^2 \rho g H/2 \frac{\cosh k(h+Z)}{\cosh k h} \sin\theta \cos\theta \; d\theta \qquad (3.13)$$

Making the substitution $Z = a \sin \theta - h$, equation (3.13) becomes

$$F_{Vmax} = \int_{-h}^{-h+a} 2\pi a^2 \rho g H/2 \frac{\cosh k (h+Z)}{\cosh k h} \frac{(Z+h)}{a} \frac{dZ}{a} \qquad (3.14)$$

Letting $u = (h+Z) k$

we have $\quad F_{Vmax} = 2\pi\rho g \; H/2 \dfrac{1}{k^2 \cosh k h} \displaystyle\int_{0}^{ak} \cosh u \; u du \quad (3.15)$

and upon carrying out the integration, equation (3.15)

yields:

$$F_{Vmax} = 2\pi\rho gH/2 \left[\frac{(ka - \sin\ ka - \cosh\ ka + 1)}{k^2\ \cosh\ k\ h} \right] \quad (3.16)$$

where $k = \frac{2\pi}{L}$

By arranging this equation in dimensionless form the vertical force coefficient becomes:

$$f_y = \frac{F_{Vmax}}{\gamma a^2 H/2} = 2\pi \left[\frac{\frac{2\pi a}{L}\ \sinh\ \frac{2\pi a}{L} - \cosh\ \frac{2\pi a}{L} + 1}{(\frac{2\pi a}{L})^2\ \cosh\ \frac{h}{a}\ \frac{2\pi a}{L}} \right]$$

$$(3.17)$$

Equation (3.17) is plotted along with equation (3.10) in Figure (13) as a function of $2\pi a/L$ for various values of h/a. These theoretical curves are also used in Chapter IV in comparison with measured vertical force data taken from both the wave force and pressure distribution models.

Evaluation of Experimental Data

Two computer programs (see Appendix I) were used to reduce the data taken from both experimental models. The hemispherical wave force model was attached to a strain gaging load cell system, which provided direct measurements of horizontal and vertical force induced by wave interaction with the hemisphere. These direct measurements

along with measurements of the period, wave height, interior pressure inside the hemisphere, and phase shift were supplied as inputs to one of the computer programs to calculate the maximum horizontal and vertical forces acting on the hemisphere. The second hemispherical model was designed to measure the instantaneous pressure distribution at various points on the surface of the shell. By inputing these instantaneous pressure distribution readings with those of corresponding wave height and phase shift readings, the second program also provided calculations of maximum horizontal and vertical wave forces.

The vertical force measured by the load cells was a result of the pressure distribution on the inside of the model as well as the external pressure distribution. Since the force resulting from the external pressure only was of interest, a correction was necessary to account for the internal pressure. As previously explained in Chapter II, the hemispherical wave force model had a small clearance above the wave channel floor so that no force would transmit through any path other than that of the strain gage load cells. As a result of this clearance the pressure inside the hemisphere fluctuated and contributed to the measured vertical force. Thus, it was necessary to locate a pressure tap indicator inside the hemisphere to measure pressure so that the vertical force

could be corrected by the amount of the interior pressure contribution. This was accomplished by use of a pressure transducer connected to the inside of the model through a hole drilled in the wave channel floor. In this way, the interior pressure contribution readings were numerically subtracted from the resultant vertical force readings taken by direct measurements. Also, in order to evaluate the maximum vertical force acting on the hemisphere, it was necessary to determine the phasing (phase shift) between the resultant and internal pressure measurements.

The vertical force (F_V) due to the pressure acting on the hemispherical wave force model at any instant in time is:

$$F_V(t) = F_R \sin \omega t - F_p \sin (\omega t + \delta) \qquad (3.18)$$

where F_R = force reading from load cells

F_p = force due to the pressure inside the hemisphere

δ = phase shift reading (between F_R & F_p)

and which, upon expanding the second term on the right hand side yields:

$$F_V(t) = (F_R - F_p \cos \delta) \sin \omega t - F_p \sin \delta \cos \omega t \qquad (3.19)$$

The amplitude of the fluctuating vertical force is then given by

$$F_V = [(F_R - F_p) \cos \delta)^2 + (F_p \sin \delta)^2]^{\frac{1}{2}} \qquad (3.20)$$

Values for these three parameters were read from the

recorder charts and equation (3.20) was used to evaluate the amplitude of the vertical force due to the external pressure distribution.

The internal pressure did not contribute to the horizontal force and, therefore, no correction was needed. Also, once the program tabulated the horizontal and vertical components of force, it was a simple matter to compute the corresponding values of force coefficients using Equations (3.10) and (3.17). Moreover, the wave length was calculated by the computer program. Initially, the deep water wave length (L_o) was used as a first approximation where:

$$L_o = 5.12 \ T^2 \quad (T=\text{period, seconds}) \qquad (3.21)$$

Then, using an iterative method, the wave length (L) was determined by:

$$L = \frac{gT^2}{2\pi} \tanh \frac{2\pi h}{L} \qquad (3.22)$$

As has already been mentioned, this investigation involved the testing of two similar submerged, hemispherical models at various water depths, wave lengths and wave heights. From the wave force model the horizontal and vertical forces were directly measured and, in order to provide a means of comparison for these force coefficients, a second hemispherical model was specially

designed to measure the instantaneous pressure distribu-
tion acting on the surface of the shell. With this
measured pressure distribution information the corres-
ponding horizontal and vertical force coefficients were
numerically determined and compared with those obtained
by direct measurements. The following expressions for
horizontal and vertical force coefficients were obtained
by integrating the instantaneous pressure distribution
over the surface area of a hemisphere as indicated in
Figure (12).
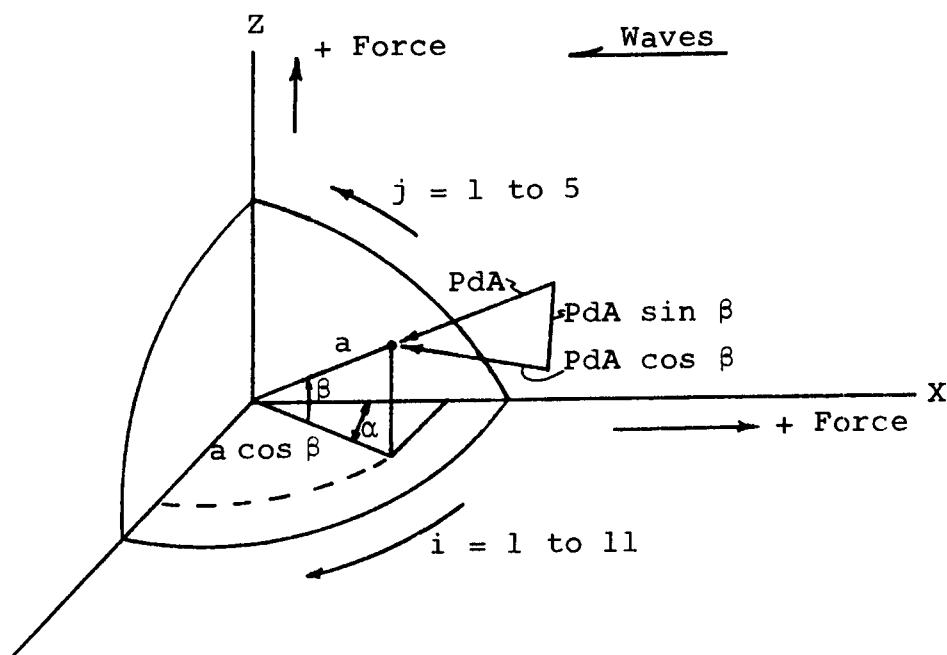
Figure 12. Quarter-section of the hemispherical
pressure distribution model.

By integrating the pressure over the surface area of the hemisphere, the following expression is obtained for horizontal force (F_H):

$$F_H(t) = - \int P \cos \beta \ dA \cos \alpha \qquad (3.23)$$

where from Figure (12) the incremental area (dA) is found to be

$$dA = a^2 \cos \beta \ d \alpha \ d \beta \qquad (3.24)$$

Substituting eq. (3.24) into (3.23) yields:

$$F_H(t) = - 2 \int_0^\pi \int_0^{\frac{\pi}{2}} P a^2 \cos \alpha \cos^2 \beta \ d \alpha \ d \beta \qquad (3.25)$$

Next, writing the expression for pressure (P) to represent the amplitude of pressure (P_0) created by corresponding amplitudes of wave height, we have

$$P(\alpha, \beta, t) = P_0(\alpha, \beta) \sin [\sigma t + \lambda(\alpha, \beta)] \qquad (3.26)$$

where $P_0(\alpha, \beta)$ = amplitude of pressure

$\lambda(\alpha, \beta)$ = phase shift angle with respect to the incident wave crest

Also $P(\alpha, \beta, t) = P_0(\alpha, \beta) [\sin \sigma t \cos \lambda + \cos \sigma t \sin \lambda] \qquad (3.27)$

Then, substituting into equation (3.26) we find

$$F_H(t) = -2a^2 \left[\int_0^\pi \int_0^{\frac{\pi}{2}} P_0(\alpha, \beta) \cos \lambda(\alpha, \beta) \cos \alpha \cos^2 \beta \ d\alpha \ d\beta \sin \sigma t + \right.$$

$$\left. \int_o^\pi \int_o^{\frac{\pi}{2}} P_o(\alpha,\beta) \sin \lambda \ (\alpha,\beta) \cos \alpha \cos^2 \beta \ d\alpha \ d\beta \cos \sigma t \right] \quad (3.28)$$

Writing the integrals occurring in equation (3.28) into summary form for computer programming purposes, we obtain:

$$F_H(t) = -2a^2[\sin \sigma t \sum_{i=1}^{10} \sum_{j=1}^{5} P_o(\alpha_i,\beta_j) \sin \lambda_{ij} \cos\alpha_i \cos^2\beta_j \Delta\alpha\Delta\beta +$$

$$\cos \sigma t \sum_{i=1}^{10} \sum_{j=1}^{5} P_o(\alpha_i,\beta_j) \cos \lambda_{ij} \cos^2\beta_j \Delta\alpha\Delta\beta] \quad (3.29)$$

Since horizontal force coefficient $f_x(t) = \dfrac{F_H(t)}{\gamma a^2 H/2} \quad (3.30)$

we have $f_x = [(2 \sum_{i=1}^{10} \sum_{j=1}^{5} (\dfrac{P_{oij}}{\gamma H/2}) \cos \lambda_{ij} \cos \alpha_i \cos^2\beta_j \Delta\alpha\Delta\beta)^2 +$

$$(2 \sum_{i=1}^{10} \sum_{j=1}^{5} (\dfrac{P_{oij}}{\gamma H/2}) \sin \lambda_{ij} \cos \alpha_i \cos^2\beta_j \Delta\alpha\Delta\beta)^2]^{\frac{1}{2}}$$
$$(3.31)$$

The derivation for the vertical force coefficient $(f_y(t))$ is the same as horizontal; except replace one $\cos\beta$ by $\sin \beta$ and remove one $\cos \alpha$. Thus,

$$f_y(t)=[(2 \sum_{i=1}^{10} \sum_{j=1}^{5} (\dfrac{P_{oij}}{\gamma H/2}) \cos \lambda_{ij} \sin \beta_j \cos \beta_j \Delta\alpha\Delta\beta)^2 +$$

$$(2 \sum_{i=1}^{10} \sum_{j=1}^{5} (\dfrac{P_{oij}}{\gamma H/2}) \sin \lambda_{ij} \sin \beta_j \cos \beta_j \Delta\alpha\Delta\beta)^2]^{\frac{1}{2}}$$
$$(3.32)$$

Also, as shown in Figure (12), the indices i and j found in Equations (3.31) and (3.32) above represent the points where the corresponding amplitudes of pressure (P_o) were measured.

Both the experimental horizontal and vertical force coefficient values computed from the above equations (Equations 3.31 and 3.32) are shown in comparison to the theoretical curves presented in Chapter IV. Also, these two equations and the ensuing Fortran program may be found in Appendix I.
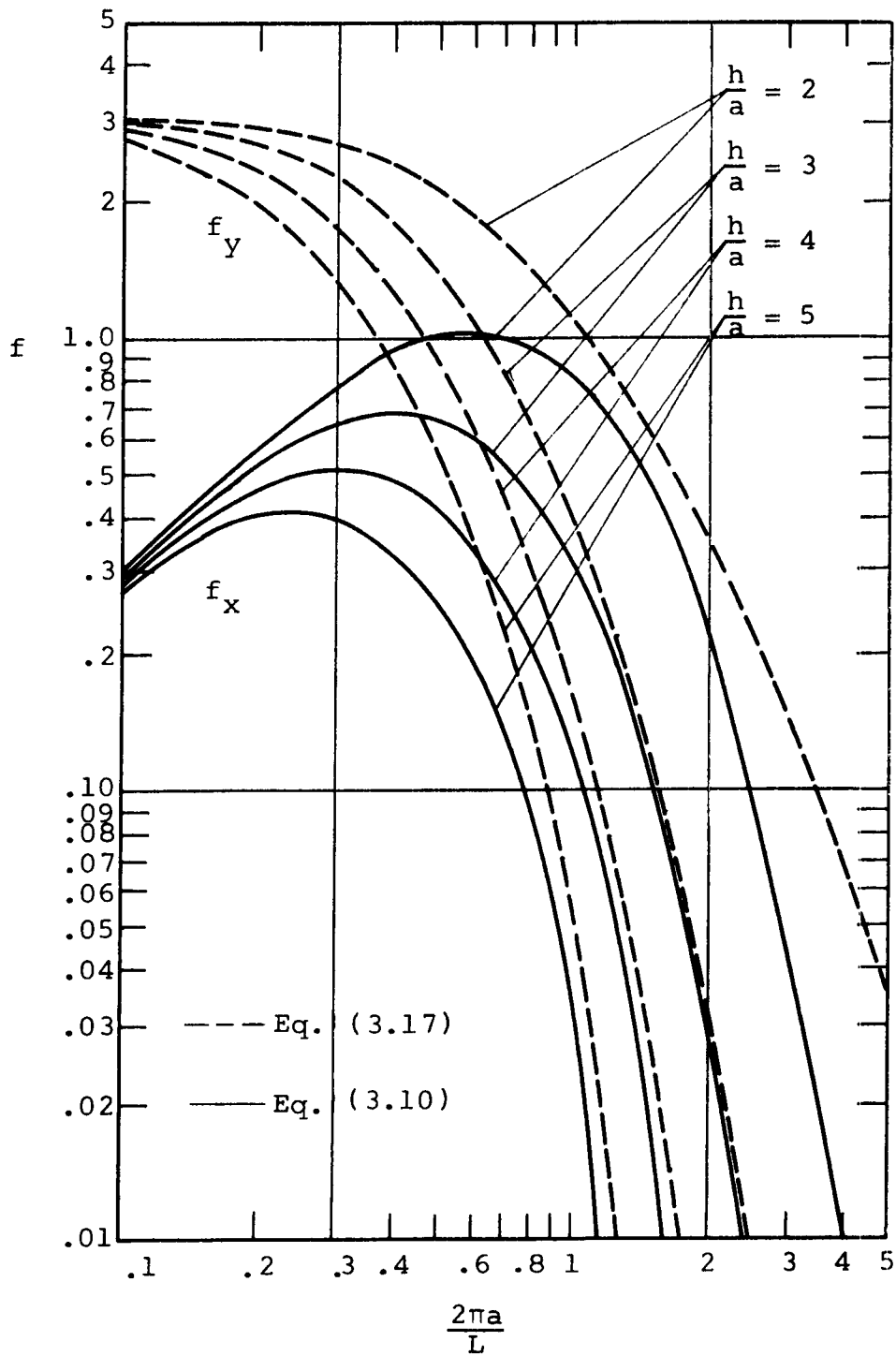
Figure 13. Horizontal and vertical force coefficients.

CHAPTER IV

PRESENTATION AND DISCUSSION OF RESULTS

The main objective of the experimental part of this research was to measure the wave induced forces acting on a hemispherical object located on the ocean floor. The results of these measurements were then compared with theories developed to predict the maximum horizontal and vertical force on large submerged structures such as oil storage tanks. Another objective was to determine the effect of wave height, wave length, water depth and size of the object both experimentally and theoretically. Therefore, in order to show these effects and to provide the comparison between experimentally measured data and corresponding theoretical calculations, the results of this study which include horizontal and vertical forces as well as pressure measurements on the surface of the hemisphere are presented in dimensionless form as a function of the wave number ($2\pi a/L$), relative water depth (h/a), and relative wave height ($H/2a$).

The work for this investigation was conducted in a two-dimensional wave channel, and the investigation involved testing two similar submerged, hemispherical models at various water depths, wave lengths and wave height. From one of these hemispherical models the direct measurements of the horizontal and vertical forces were taken

and presented in the form of horizontal and vertical force

coefficients (See Appendix II). Whereas, from the second

model, measurements of the instantaneous pressure acting

on its surface were made and, with this information, the

net horizontal and vertical force coefficients were numer-

ically evaluated by use of Equations (3.31) and (3.32) and

compared with the coefficients obtained by the direct

force measurements. A comparison between the theoretical

force coefficients obtained from Equations (3.10) and

(3.17) and experimentally determined values are presented

in Figures (14-21).

It is well known that the excursion dimensions of

fluid particles under gravity waves are proportional to

the wave height and, the ratio of wave height to object

size is an important parameter with regard to viscous ef-

fects. Since this parameter was kept small in the case

of this experimental investigation, the amplitude of the

fluid motion was small compared to the object size. There-

fore, viscous effects for this investigation were negli-

gible because the fluid must travel a distance of the

order of half a diameter before the trailing vortices

develop and separation sets in. However, in order to

avoid using any experimental data which may have been sub-

jected to viscous effects, dimensionless parameters of

maximum horizontal and vertical force versus relative wave
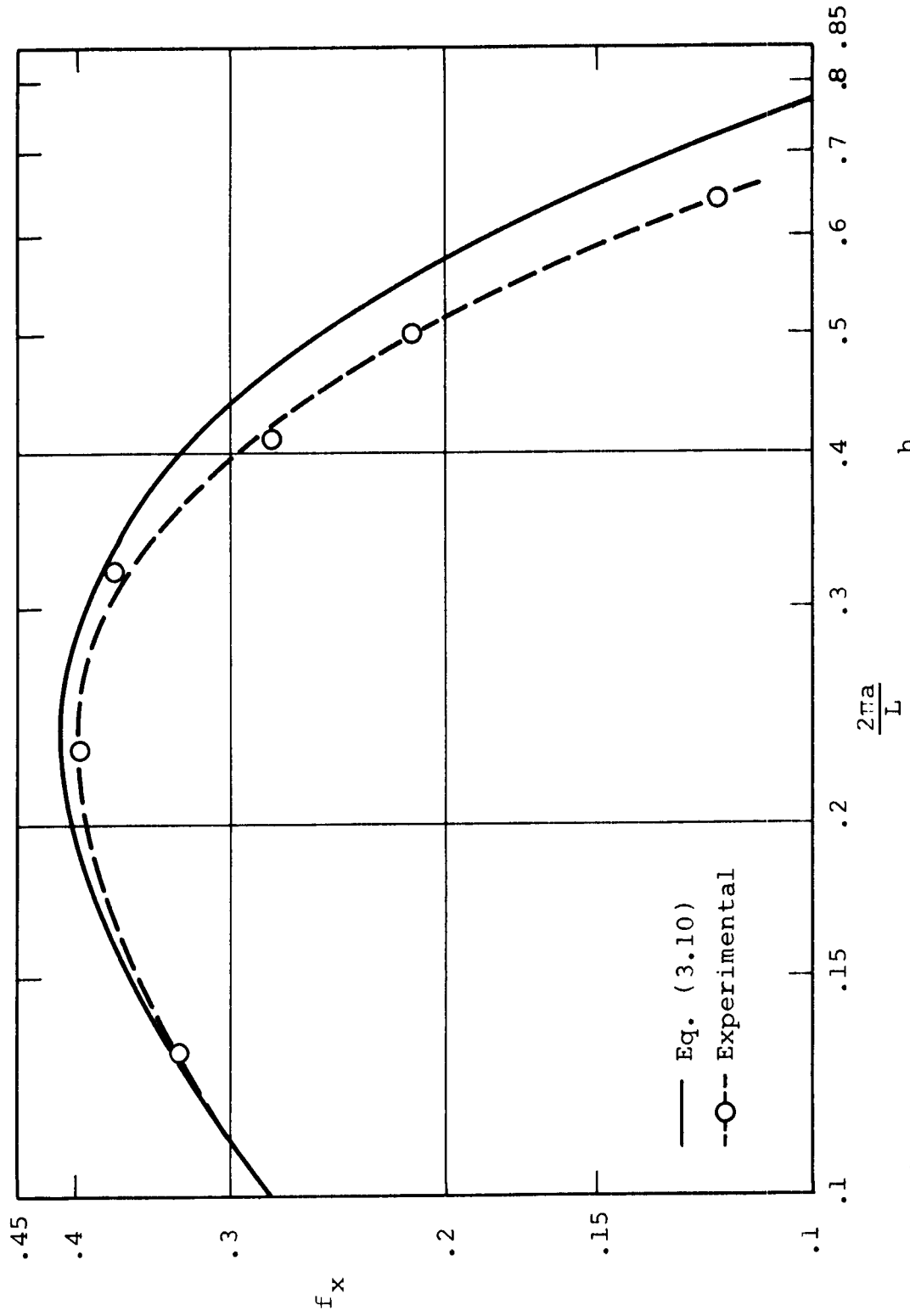
Figure 14. Horizontal force coefficient for $\frac{h}{a} = 5$.
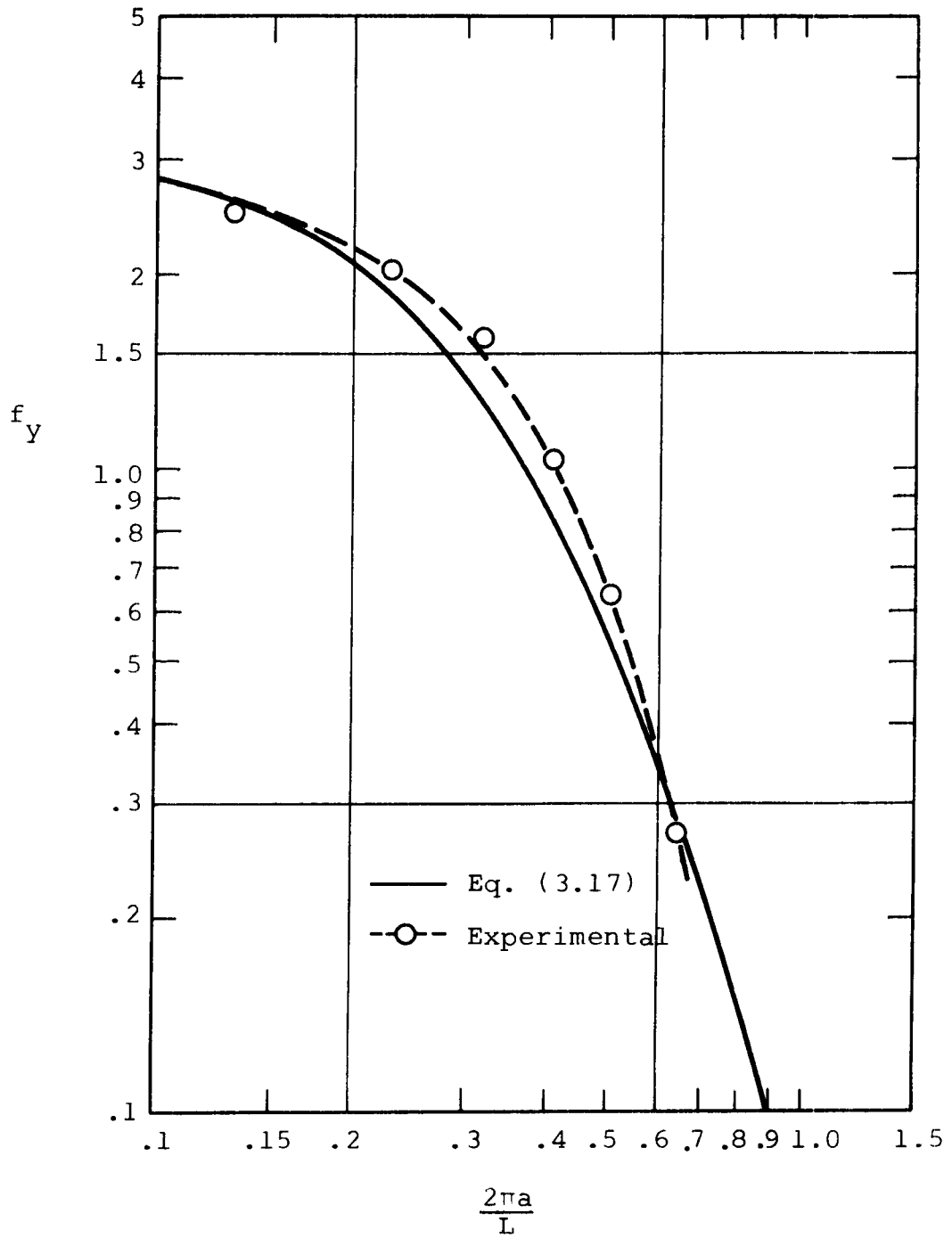
Figure 15. Vertical force coefficient for $\frac{h}{a} = 5$.
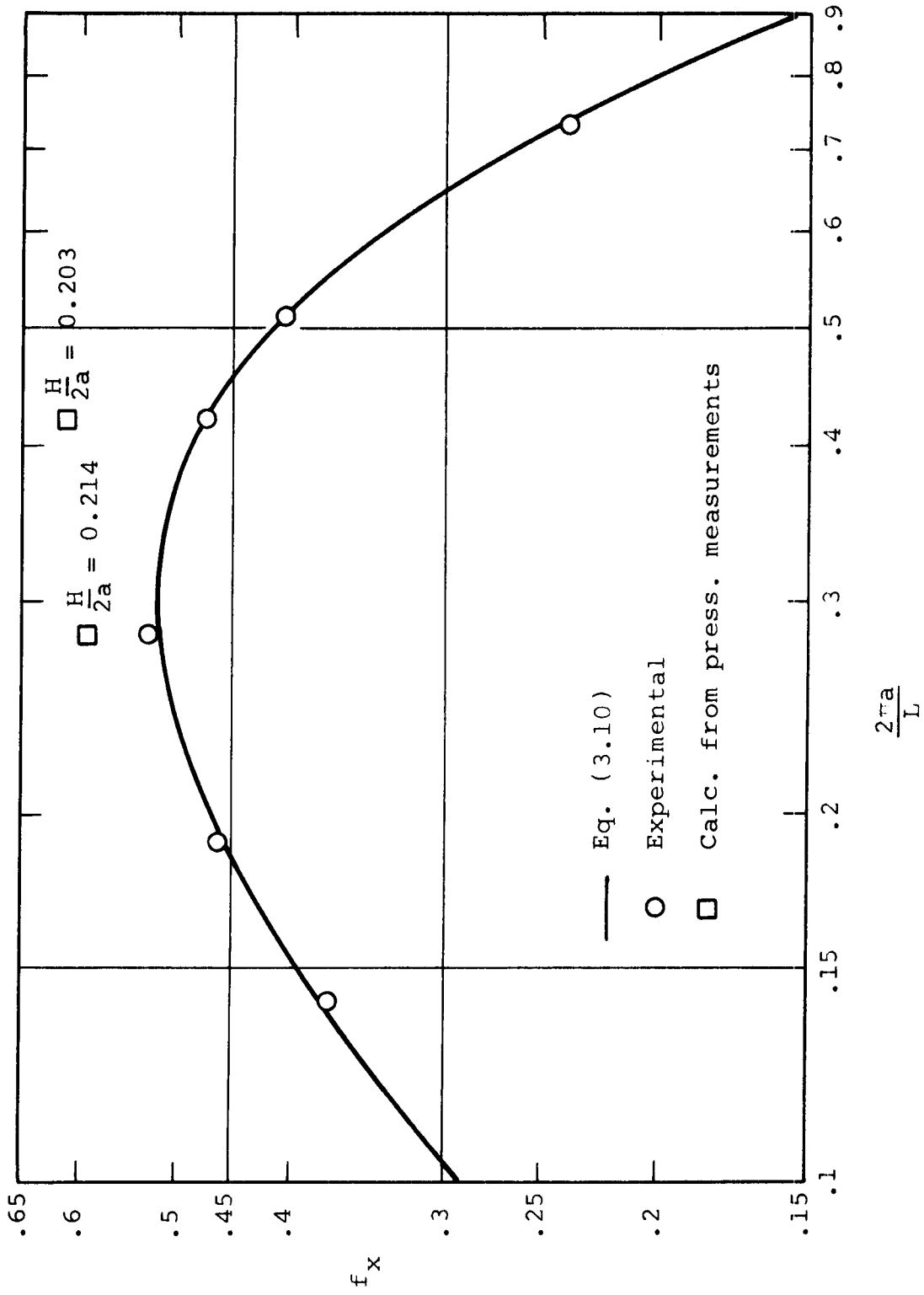
Figure 16. Horizontal force coefficient for $\frac{h}{a} = 4$.
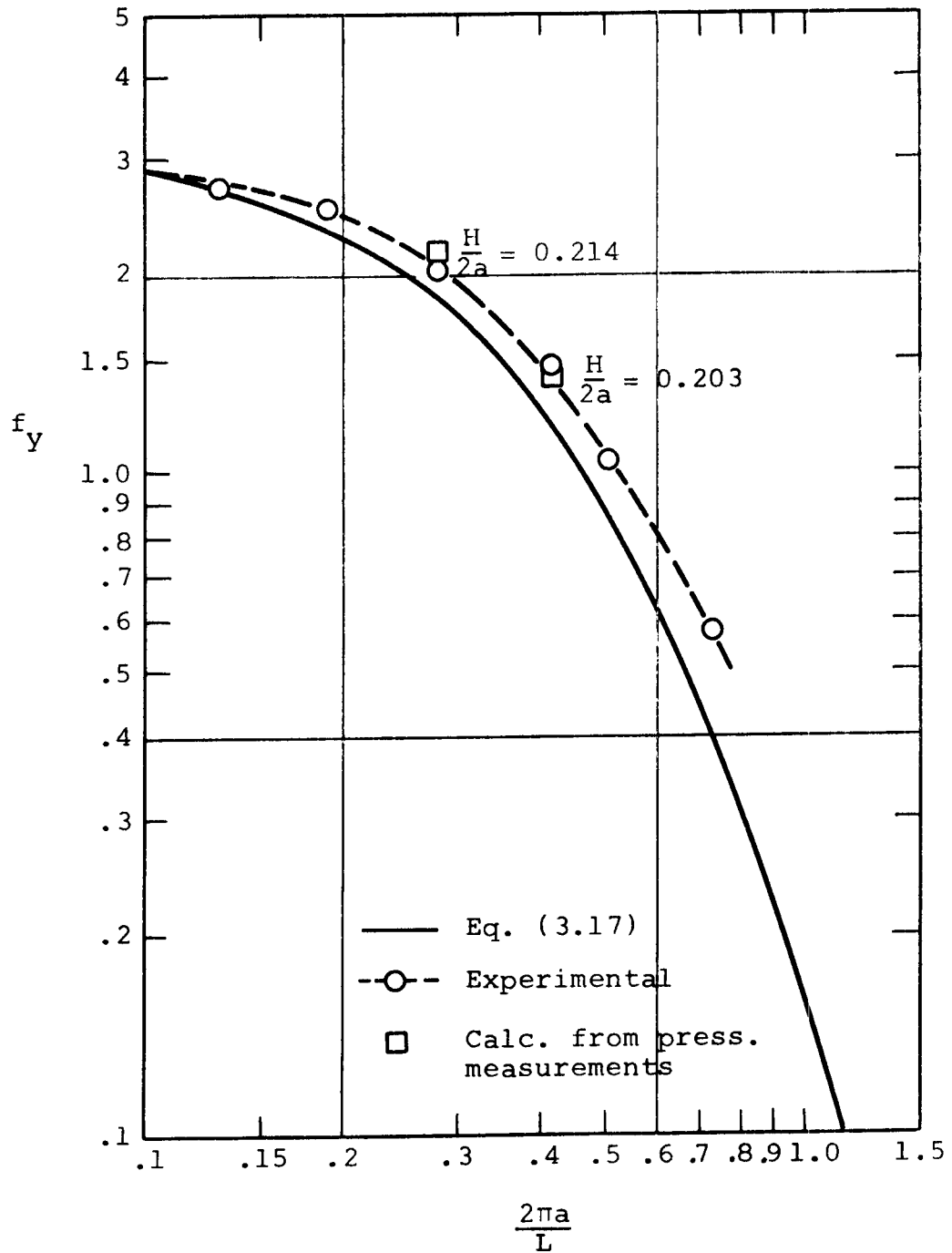
Figure 17. Vertical force coefficient for $\frac{h}{a} = 4$.
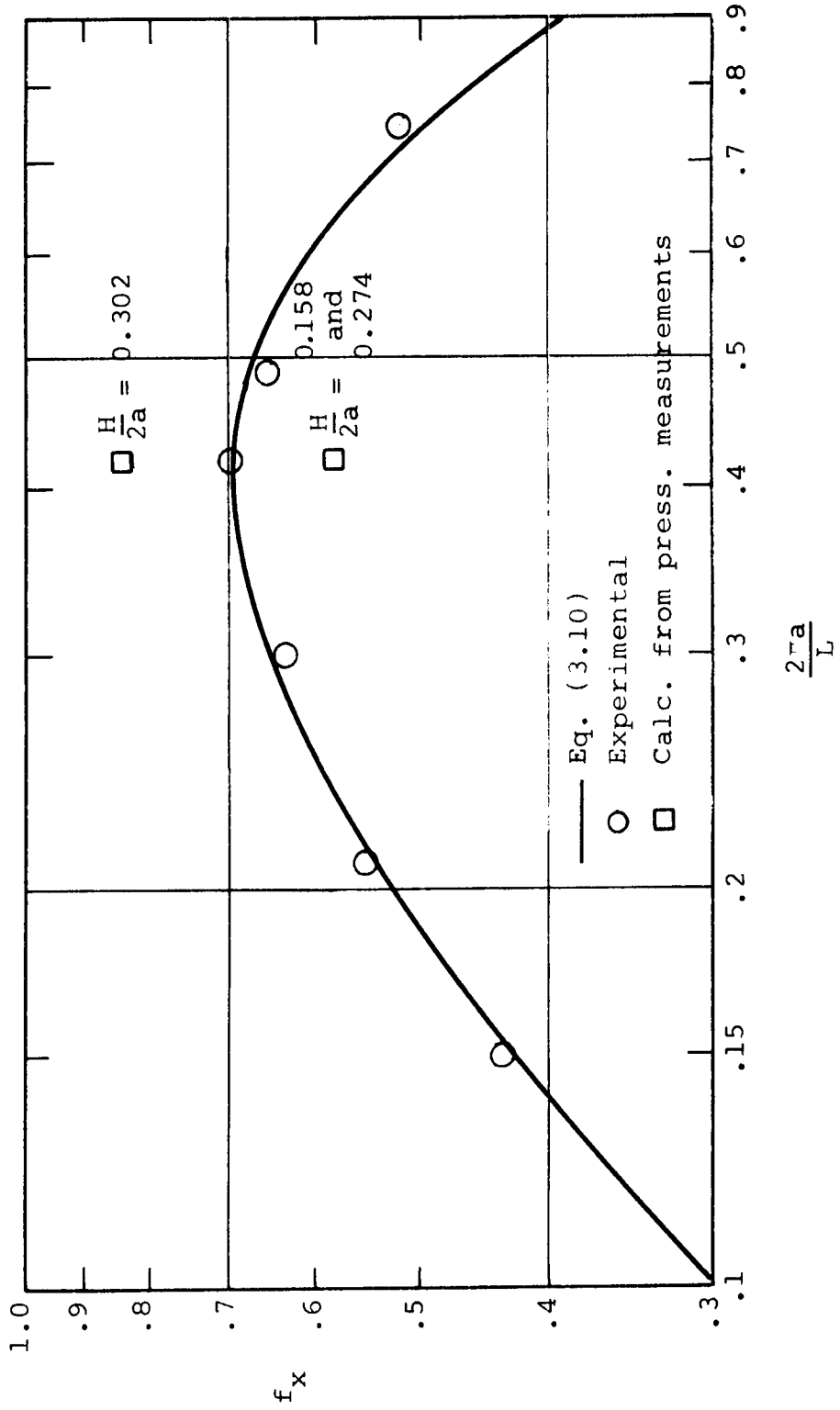
Figure 18. Horizontal force coefficient for $\frac{h}{a} = 3$.
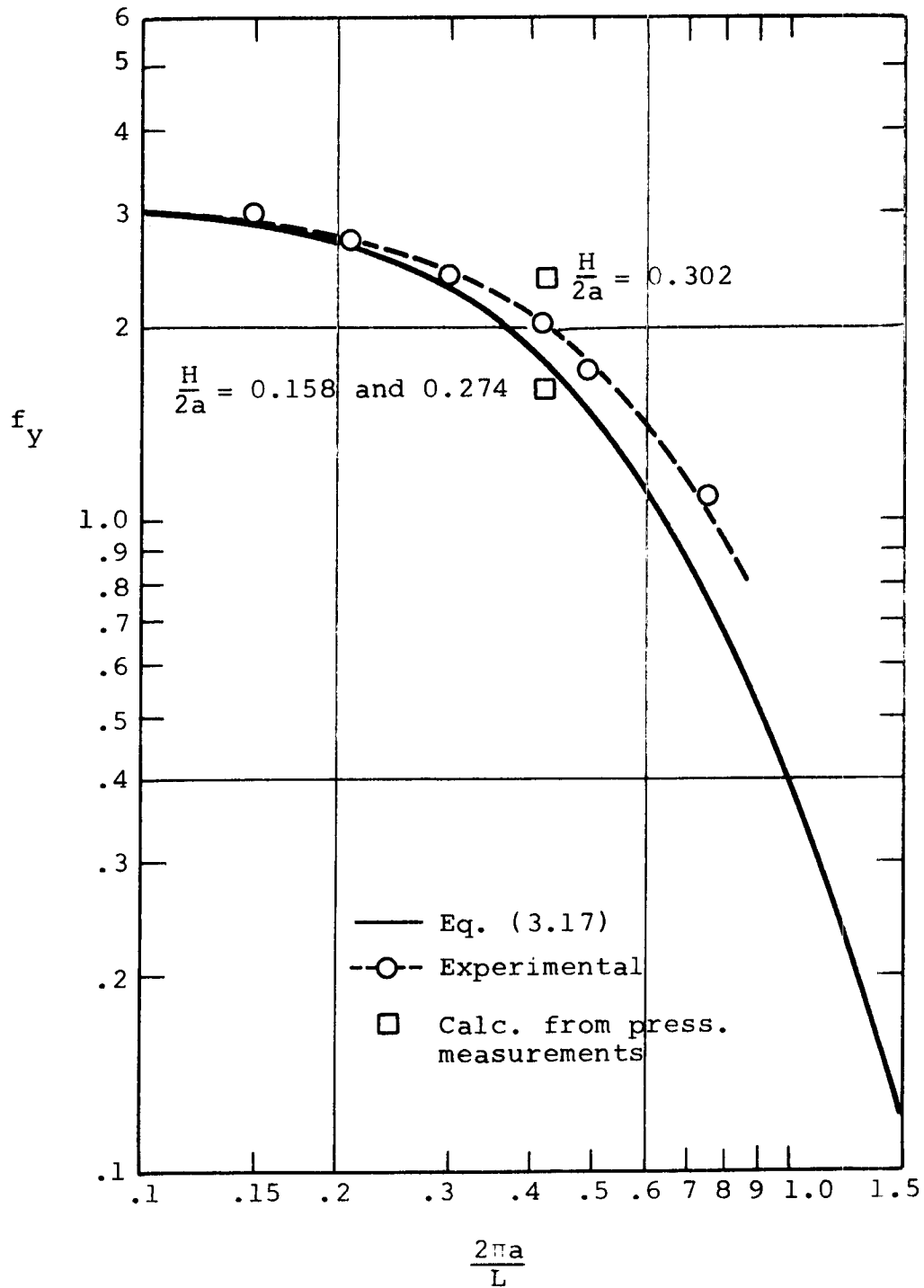
Figure 19. Vertical force coefficient for $\frac{h}{a} = 3$.
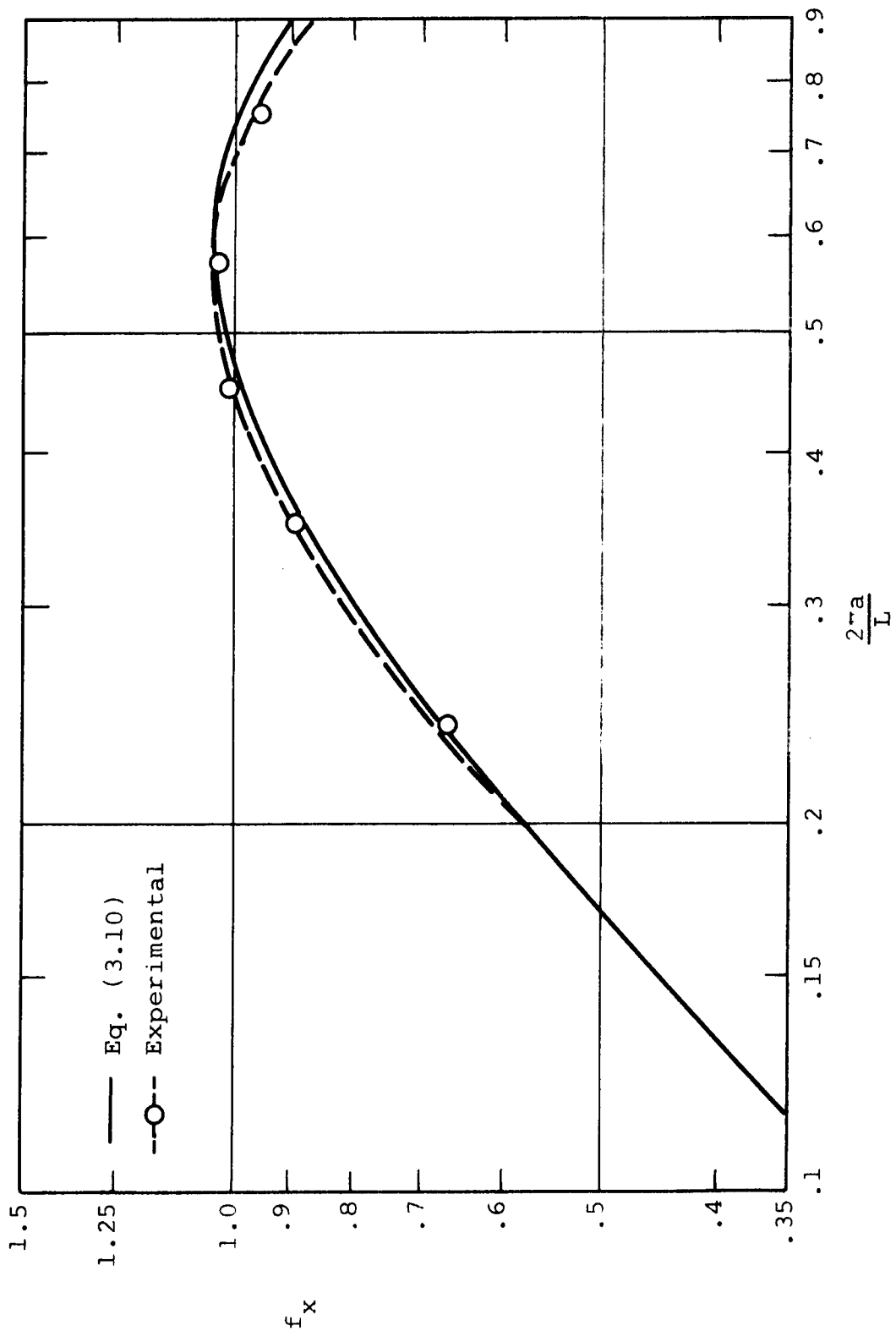
Figure 20. Horizontal force coefficient for $\frac{h}{a} = 2$.
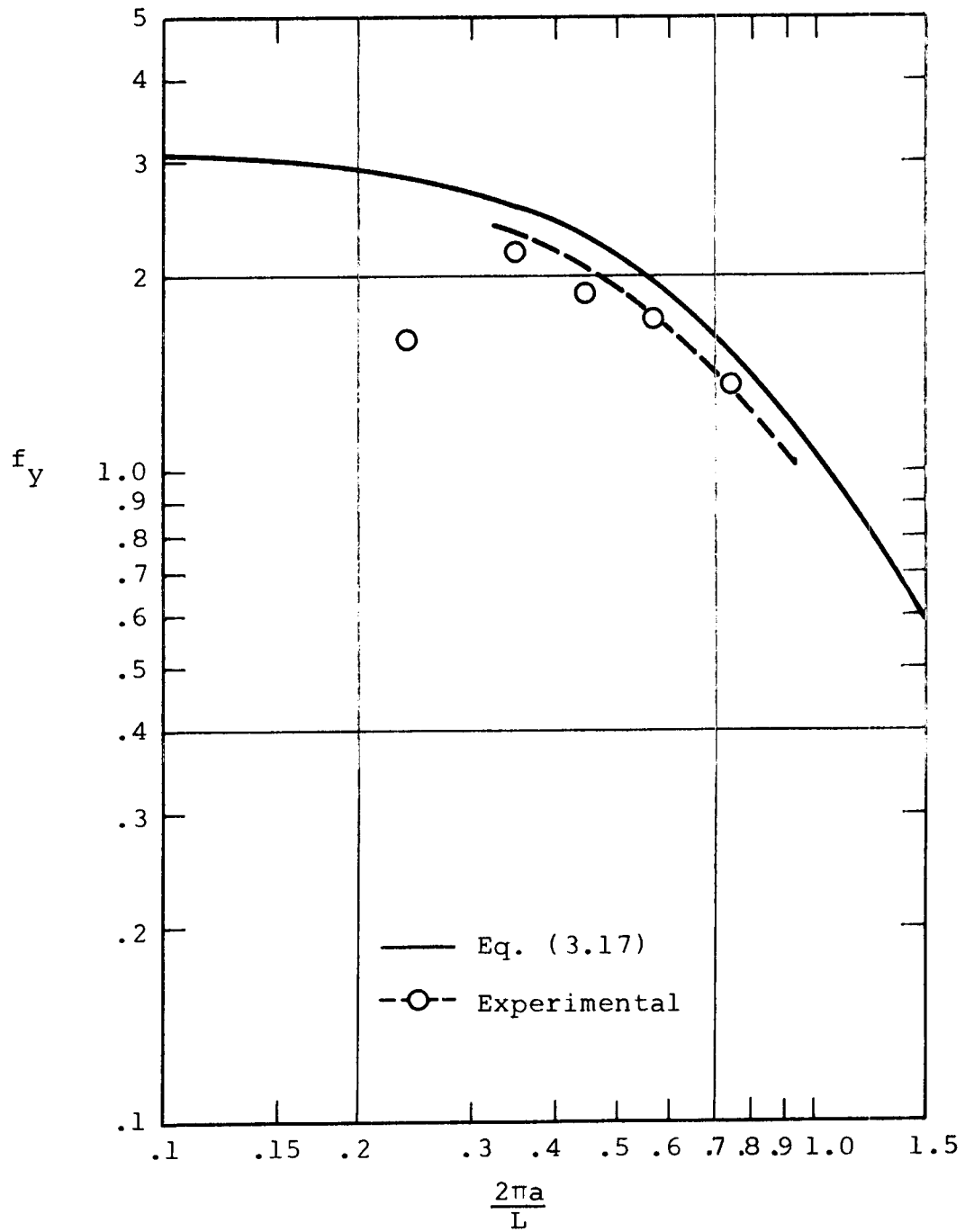
Figure 21. Vertical force coefficient for $\frac{h}{a} = 2$.

height were plotted (See Appendix III) as shown in Figures
(22-29) (See Appendix IV) for various ratios of relative
water depth. As can be seen in these figures, linear
slopes were drawn to distinguish the transitional points
where viscous effects would become important and, hence,
where the experimental data would diverge from the pro-
posed theory. From these linear slopes horizontal and
vertical force coefficients were obtained (See Appendix
V) and plotted in comparison to the theories represent
by Figures (14-21).

Evaluation of Results

In general, the correlation between the force coef-
ficient values obtained from direct force and pressure
distribution measurements to those obtained from the the-
oretical analysis compared favorably. However, the cor-
relation of the horizontal force coefficient data was
found to be in better agreement with the developed theory
(Equation 3.10) than that of the vertical force coef-
ficient data to its proposed theory (Equation 3.17).

Essentially, as can be seen in Figures (14-21), both
the experimentally determined horizontal and vertical
force coefficient data points follow the same general path
as that of their theoretical counterparts. Also, these
experimental points can be seen to converge to the theory

as the wave length increases in size, i.e., decrease in wave number ($2\pi a/L$). This convergence to the theory for small values of $2\pi a/L$ follows the other basic assumption made in the development of the theories that if the object size to wave length is small, the incident wave will not be scattered upon encountering a large object. However, with the decrease in wave length, the ratio of object size to wave length increases, thereby, making the reflection of the incident wave more prominent until eventually the wave is scattered. In the instance of this investigation, as the wave number increased in magnitude, reflections also increased in magnitude which caused the experimental data to diverge from the developed theories.

In order to avoid selecting experimental horizontal or vertical force coefficient data which may or may not be subject to viscous effects due to the increase in wave height, one composite coefficient value was determined for each wave length and corresponding range of wave heights. This was accomplished through the use of Figures (22-29) where the effects of each group of wave heights are depicted as a function of maximum wave force and relative wave height. As can be seen from these curves, the apparent transitional separation points are distinguishable by the divergence of the curves from the linear variation. The values of these slopes in the linear region were then

used to provide composite horizontal or vertical force coefficient data plotted in Figures (14-21).

The composite values of horizontal force coefficient data obtained from Figures 22, 24, 26, and 28 for each wave number plotted in Figures (14-21) are all, as would be expected, similar in nature. The initial data points plotted for the smallest values of wave number in all cases agree very well with the theoretical curves. Also, each data point plotted against the largest value of wave number was found to be further from the theoretical curves than those plotted for lesser values of wave number. This behavior of the experimental results is very much as expected since one of the basic assumptions upon which the theory is based requires $2\pi a/L$ to be small.

In regard to the composite values of vertical force coefficient data obtained from Figures 23, 25, 27, and 29, three of the four initial data points agreed with the theoretical curves. However, in the case of the shallowest experimental depth (d=7"), the force coefficient is well below the predicted theory. Here, the force coefficient corresponding to the smallest of $2\pi a/L$ plotted in Figure (21) is probably the result of the shallow water depth affecting the wave shape (any wave diverging from the assumed linear sinusoidal pattern will cause a divergence from the theory). Also, as can be seen for the three

higher cases of relative water depth, the vertical force coefficient theory gets increasing lower in relation to the experimental data with the increase in wave number.

The horizontal and vertical force coefficients obtained from the measured pressure distribution vary to some degree with the theory. As can be seen in Figures (16) and (17), both sets of horizontal and vertical data points are above their corresponding theories. Whereas, the force coefficient points in Figures (18) and (19) are found to straddle the theory. These marked differences in both the above cases can only be attributed to some unknown experimental error. Therefore, in view of these variances in the force coefficients obtained from the pressure distribution model tests, it is suggested that future model tests be carried out using similar experimental procedures and using Equations (3.31) and (3.32) to evaluate the data. It is also suggested that conducting the tests in a three-dimensional tank may eliminate any possible errors induced by reflections from a two-dimensional wave channel testing facility.

Conclusions

The main objective of this research was to develop and validate both a maximum horizontal and vertical wave force theory which would predict wave forces for large

submerged structures such as oil storage tanks. On the basis of the theoretical and experimental results presented herein, the following conclusions are warranted:

1. Viscous effects can be neglected and a linear relationship exists between the force and wave height as long as the relative displacement of the fluid particles is small.

2. The horizontal force coefficient agrees well with the theory over the range of values of $2\pi a/L$ tested.

3. Equation 3.17 predicts values of the vertical force coefficient which are smaller than the experimental, the curves tending to diverge at increasing values of $2\pi a/L$.

4. The vertical force coefficient is a monotonically decreasing function of $2\pi a/L$ while the horizontal force coefficient shows a maximum at values of $2\pi a/L$ depending on the relative depth (h/a).

BIBLIOGRAPHY

(1) Blagoveshchensky, S. N., "Theory of Ship Motions",
    Vol. I, Dover Publications, Inc., 1962, p. 16.

(2) Brater, E. F., McNown, J. S., Stair, L. D., "Wave
    Forces on Submerged Structures", J. Hyd. Div.
    ASCE, Paper 1833, 84, Hy 6, November 1958.

(3) Garrison, C. J., "Unpublished Notes on Wave Inter-
    action with Large Submerged Structures", 1969.

(4) Grace, G. A., and Casciano, F. M., "Ocean Wave
    Forces On A Subsurface Sphere", J. Waterways
    and Harbor Div., Paper 6722, n ww3, August 1969,
    pp. 291-317.

(5) Harleman, D. R. F., and Shapiro, W. C., "Investiga-
    tion on the Dynamics of Moored Structures in
    Waves", Proc. Seventh Conf. Coastal Eng., Chap.
    41, 1961, pp. 746-765.

(6) Lamb, Sir Horace, "Hydrodynamics", 6th Ed. New York:
    Dover Publications, Inc., 1945.

(7) Morison, J. R., Johnson, J. W., and O'Brien, M. P.,
    "Experimental Studies of Forces on Piles",
    Proc. Fourth Conf. Coastal Council on Wave Re-
    search, Berkeley, Calif.: The Engineering
    Foundation Council on Wave Research, 1954,
    pp. 340-370.

(8) O'Brien, M. P., and Morison, J. R., "The Forces
    Exerted By Waves on Objects", Trans. Amer.
    Geophys. Union, v 33 n 1, February 1952, pp.
    32-38.

(9) Sarpkaya, T., and Garrison, C. J., "Vortex Forma-
    tion and Resistance in Unsteady Flow", J. of
    Applied Mechanics, Trans. ASME, March 1963.

(10) Stokes, G. G., "Collected Papers Vol. I", Trans.
     Camb. Phil. Soc. vol. 8, 1843, p. 17.

APPENDICES

APPENDIX I

COMPUTER PROGRAMS

No. 1 Fortran program for evaluating data taken from the wave force model.

No. 2 Fortran program for evaluating data taken from the pressure distribution model.

```
No. 1
C      THIS PROGRAM IS FOR WAVE FORCE DATA REDUCTION FOR HEMISPHERICAL TANKS
C      A=TANK RADIUS,FT.
C      DEPTH=WATER DEPTH,FT.
C      CALWH=WAVE HEIGHT CALIBRATION COEF, FT./MM
C      CALV=VERTICAL FORCE CALIBRATION COEF, GM/MM
C      CALH=HORIZONTAL FORCE CALIBRATION COEF, GM/MM
C      CALP=PRESSURE CALIBRATION COEF, FT.WATER/MM
C      N=NUMBER OF RUNS
C      CSPEED=CHART SPEED, MM/SEC.
C      OUTPUT DATA
C      NO=RUN NUMBER
C      WL=WAVE LENGTH,FT.
C      T=PERIOD,SEC.
C      WAVENO=2*PI*A/L,WAVE NUMBER
C      RELDEP=RELATIVE DEPTH=D/L
C      RELWH=RELATIVE WAVE HEIGHT=H/2A
C      FH=HORIZONTAL FORCE COEF
C      FV=VERTICAL FORCE COEF
       A=3.5/12.
       DEPTH=17.5/12.
       G=32.17
       PI=3.1416
       CALWH=.00435
        CALV=2.817
       CALH=5.125
       CALP=.003335
       N=13
       WRITE(6,10) A,DEPTH,CALWH,CALV,CALH,CALP
 10    FORMAT(5X2H4=F5.3,4X6HDEPTH=F5.2,4X6HCALWH=F8.6,4X5HCALV=F6.2,4X5H
      1CALH=F6.2,4X5HCALP=F6.4)
       I=0
 13    READ(5,15)  NO,CSPEED,PERIOD,WAVEH,FORCEV,FORCEH,PRESS,SHIFT
```

No. 1 (continued)

```
15 FORMAT(I3,    7(2X,F5.1))
   I=I+1
   CALT=1./CSPEED
   T=CALT*PERIOD
   WL=G/(2.*PI)*T**2
11 WL=G*T**2/2./PI*TANH(2.*PI*DEPTH/WL)
   WL1=WL
   WL=G*T**2/2./PI*TANH(2.*PI*DEPTH/WL)
   WL2=WL
   IF(ABS(WL2-WL1)-.001) 12,12,11
12 CONTINUE
   WAVENO=2.*PI*A/WL
   RELDEP=DEPTH/WL
   H=CALWH*WAVEH
   RELWH=H/2./A
   FH=CALH/454.*FORCEH/2./(62.4*A**2*H/2.)
   FP=CALP*PRESS*62.4*PI*A**2
   FVR=CALV/454.*FORCEV
   PHASE=2.*PI*SHIFT/PERIOD
   FFV=SQRT((FVR-FP*COS(PHASE))**2+(FP*SIN(PHASE))**2)
   FV=FFV/2./(62.4*A**2*H/2.)
   WRITE(6,18)NO,CSPEED,PERIOD,WAVEH,FORCEV,FORCEH,PRESS,SHIFT
18 FORMAT(3HNO=I3,3X7HCSPEED=F5.1,3X7HPERIOD=F5.1,3X6HWAVEH=F6.2,3X7H
  1FORCEV=F5.1,3X7HFORCEH=F5.1,3X6HPRESS=F5.1,3X6HSHIFT=F5.1)
   WRITE(6,20)NO,WL,T,WAVENO,RELDEP,RELWH,FH,FV
20 FORMAT(1X3HNO=I3,3X3HWL=F5.2,               3X2HT=F5.2,3X7HWAVENO=
  1F5.2,3X7HRELDEP=F5.2,3X6HRELWH=F6.3,3X3HFH=F5.2,3X3HFV=F5.2)
   IF(I-N) 13,14,14
14 CONTINUE
   STOP
   END
```

No. 2

```
C    THIS PROGRAM IS FOR PRESS. DISTRIBUTION DATA REDUTION FOR A
C    HEMISPHERICAL OIL STORAGE TANK MODEL
C    DELBAT=(PI/2)/5=PI/10=.31416
C    CALP=PRESSURE CALIBRATION COEF. FT. WATER/MM
C    WL=DISTANCE BETWEEN CRESTS,MM
C    CALLAM=2*PI/WL
C    WH=WAVE HEIGHT,FT.
C    DEPTH=DISTANCE BETWEEN SWL AND TANK BOTTOM,FT.
C    PERIOD=TIME LAPS BETWEEN WAVE CRESTS,SEC.
C    R=TANK RADIUS,FT.
C    RELWH=RELATIVE WAVE HEIGHT=WH/2R
C    WAVFL= WAVE LENGTH,FT
     DIMENSION PRESS(11,5),XLAMD(11,5),PRESS(11,5),XLAM(11,5)
    1,CALP(11,5)
     A=7
     B=2
     C=0
     D=0
     DELBAT=.31416
     WL=26.5
     CALLAM=6.2832/WL
     WH=.176
     DEPTH=13.5/12.
     PERIOD=1.66
     R=3.5/12.
     RELWH=WH/2./R
     WAVEL=4.72
     WRITE(6,6)  WAVEL,DEPTH,PERIOD,RELWH
  6  FORMAT(F5.2,3XF5.2,3XF6.2,3XF6.3)
     READ(5,10)((PRESSO(I,J),I=1,11),J=1,5)
 10  FORMAT(11(F5.1,5X))
     READ(5,10)((XLAMD(I,J),I=1,11),J=1,5)
```

```
No. 2 (continued)
   11 FORMAT(11(F5.1,1X))
      READ (5,12) ((CALP(I,J),I=1,11),J=1,5)
   12 FORMAT (11(F6.5))
      DO 50 J=1,5
      DO  50 I=1,11
      IF(I-1)2,2,3
    2 DELALP=.31416/2.
      GO TO 8
    3 IF (I-11)4,2,2
    4 DELALP=.31416
    8 CONTINUE
      ALPH(I)=.31416*FLOAT(I-1)
      BAT(J)=.31416*FLOAT(J)-.31416/2.
      PRESS(I,J)=CALP(I,J)*PRESSD(I,J)/WH
      XLAM(I,J)=CALLAM*XLAMD(I,J)
      WRITE(6,70)J,I,PRESSD(I,J),XLAMD(I,J),PRESS(I,J),XLAM(I,J)
   70 FORMAT(I3,2XI3,5XF5.1,2XF5.1,5XF6.3,2XF6.3)
      TER=2.*PRESS(I,J)*COS(XLAM(I,J))*COS(ALPH(I))*(COS(BAT(J))**2)*
     1DELALP*DELBAT
      A=A+TER
      B=B+TER*TAN(XLAM(I,J))
      TER=2.*PRESS(I,J)*COS(XLAM(I,J))*SIN(BAT(J))*COS(BAT(J))*DELALP*
     1DELBAT
      C=C+TER
   50 D=D+TER*TAN(XLAM(I,J))
      FH=SQRT(A**2+B**2)
      FV=SQRT(C**2+D**2)
      PHASEH=ATAN(B/A)
      PHASEV=ATAN(D/C)
      WRITE(6,50) FH,FV,PHASEH,PHASEV
   50 FORMAT(F5.3,3XF6.3,3XF5.2,3XF5.2)
      STOP
      END
```

APPENDIX II

WAVE FORCE MODEL DATA

Run No. 1 - 33:   Depth = 17.5 inches

Run No.	L (ft)	T (Sec)	$\frac{2\pi a}{L}$	$\frac{d}{L}$	$\frac{H}{2a}$	f_x	f_y
1	14.14	2.20	0.13	0.10	0.053	0.31	2.15
2	14.14	2.20	0.13	0.10	0.101	0.32	2.50
3	14.14	2.20	0.13	0.10	0.157	0.34	2.41
4	14.14	2.20	0.13	0.10	0.207	0.33	2.61
5	14.14	2.20	0.13	0.10	0.261	0.34	2.55
6	8.13	1.40	0.23	0.18	0.075	0.37	2.11
7	8.13	1.40	0.23	0.18	0.151	0.41	2.08
8	8.13	1.40	0.23	0.18	0.227	0.40	2.03
9	8.13	1.40	0.23	0.18	0.304	0.40	2.01
10	8.13	1.40	0.23	0.18	0.369	0.39	2.01
11	5.71	1.10	0.32	0.26	0.099	0.35	1.60
12	5.71	1.10	0.32	0.26	0.190	0.38	1.67
13	5.71	1.10	0.32	0.26	0.284	0.38	1.64
14	5.71	1.10	0.32	0.26	0.361	0.39	1.62
15	4.47	0.95	0.41	0.33	0.107	0.27	1.00
16	4.47	0.95	0.41	0.33	0.206	0.28	1.02
17	4.47	0.95	0.41	0.33	0.301	0.29	1.05
18	4.47	0.95	0.41	0.33	0.368	0.32	1.04
19	3.65	0.85	0.50	0.40	0.116	0.21	0.68
20	3.65	0.85	0.50	0.40	0.197	0.22	0.65
21	3.65	0.85	0.50	0.40	0.262	0.22	0.64
22	3.65	0.85	0.50	0.40	0.310	0.23	0.60
23	3.65	0.85	0.50	0.40	0.343	0.24	0.62
25	2.87	0.75	0.64	0.51	0.133	0.11	0.25
26	2.87	0.75	0.64	0.51	0.183	0.12	0.25
27	2.87	0.75	0.64	0.51	0.210	0.13	0.27
28	2.87	0.75	0.64	0.51	0.239	0.13	0.28
29	20.57	3.10	0.09	0.07	0.066	0.22	1.90
31	20.57	3.10	0.09	0.07	0.127	0.27	1.83
33	20.57	3.10	0.09	0.07	0.197	0.28	2.01

Run No. 39 - 69: Depth = 14.0 inches

Run No.	L (ft)	T (Sec)	$\frac{2\pi a}{L}$	$\frac{d}{L}$	$\frac{H}{2a}$	f_x	f_y
39	13.45	2.30	0.14	0.09	0.075	0.31	2.69
40	13.45	2.30	0.14	0.09	0.109	0.34	2.81
41	13.45	2.30	0.14	0.09	0.158	0.39	2.70
42	13.45	2.30	0.14	0.09	0.186	0.40	2.97
43	13.45	2.30	0.14	0.09	0.207	0.41	3.25
44	13.45	2.30	0.14	0.09	0.255	0.41	3.00
45	9.55	1.70	0.19	0.12	0.055	0.43	2.58
46	9.55	1.70	0.19	0.12	0.118	0.44	2.61
47	9.55	1.70	0.19	0.12	0.147	0.47	2.56
48	9.55	1.70	0.19	0.12	0.223	0.49	2.66
49	9.55	1.70	0.19	0.12	0.215	0.50	2.67
50	9.55	1.70	0.19	0.12	0.298	0.50	2.70
51	6.49	1.25	0.28	0.18	0.067	0.49	2.03
52	6.49	1.25	0.28	0.18	0.149	0.51	2.12
53	6.49	1.25	0.28	0.18	0.215	0.53	2.08
54	6.49	1.25	0.28	0.18	0.283	0.53	2.16
55	6.49	1.25	0.28	0.18	0.317	0.55	2.15
56	4.32	0.95	0.42	0.27	0.085	0.50	1.46
57	4.32	0.95	0.42	0.27	0.185	0.46	1.40
58	4.32	0.95	0.42	0.27	0.252	0.48	1.50
59	4.32	0.95	0.42	0.27	0.294	0.49	1.55
60	4.32	0.95	0.42	0.27	0.347	0.50	1.58
61	3.58	0.85	0.51	0.33	0.103	0.36	1.03
62	3.58	0.85	0.51	0.33	0.186	0.40	1.06
63	3.58	0.85	0.51	0.33	0.244	0.42	1.11
64	3.58	0.85	0.51	0.33	0.298	0.44	1.23
65	3.58	0.85	0.51	0.33	0.308	0.47	1.27
66	2.49	0.70	0.73	0.73	0.101	0.23	--
67	2.49	0.70	0.73	0.47	0.165	0.26	0.58
68	2.49	0.70	0.73	0.47	0.214	0.26	0.59
69	2.49	0.70	0.73	0.47	0.223	0.27	0.62

Run No. 55A - 69A, 70 - 83:   Depth = 10.5 inches

Run No.	L (ft)	T (Sec)	$\frac{2\pi a}{L}$	$\frac{d}{L}$	$\frac{H}{2a}$	f_x	f_y
55A	12.34	2.40	0.15	0.07	0.048	0.41	3.27
56A	12.34	2.40	0.15	0.07	0.087	0.44	2.63
57A	12.34	2.40	0.15	0.07	0.106	0.44	3.19
61A	8.74	1.75	0.21	0.10	0.056	0.30	2.60
62A	8.74	1.75	0.21	0.10	0.114	0.45	2.35
63A	8.74	1.75	0.21	0.10	0.176	0.54	2.48
64A	8.74	1.75	0.21	0.10	0.207	0.57	2.81
65A	8.74	1.75	0.21	0.10	0.275	0.57	2.48
66A	6.16	1.30	0.30	0.14	0.075	0.58	2.33
67A	6.16	1.30	0.30	0.14	0.146	0.64	2.37
68A	6.16	1.30	0.30	0.14	0.210	0.62	2.47
69A	6.16	1.30	0.30	0.14	0.226	0.58	2.51
70	4.36	1.00	0.42	0.20	0.074	0.66	2.13
71	4.36	1.00	0.42	0.20	0.156	0.74	2.01
72	4.36	1.00	0.42	0.20	0.216	0.66	2.07
73	4.36	1.00	0.42	0.20	0.267	0.68	2.10
74	3.73	0.90	0.49	0.23	0.087	0.49	1.64
75	3.73	0.90	0.49	0.23	0.158	0.65	1.72
76	3.73	0.90	0.49	0.23	0.224	0.66	1.78
77	3.73	0.90	0.49	0.23	0.267	0.64	1.78
78	2.45	0.70	0.75	0.36	0.085	0.47	1.12
79	2.45	0.70	0.75	0.36	0.157	0.53	1.29
80	2.45	0.70	0.75	0.36	0.218	0.54	1.21
81	2.45	0.70	0.75	0.36	0.085	0.47	1.04
82	2.45	0.70	0.75	0.36	0.163	0.54	1.02
83	2.45	0.70	0.75	0.36	0.218	0.54	1.04

Run No. 89 - 115:   Depth = 7.0 inches

Run No.	L (ft)	T (Sec)	$\frac{2\pi a}{L}$	$\frac{d}{L}$	$\frac{H}{2a}$	f_x	f_y
89	7.73	1.85	0.24	0.08	0.040	0.67	1.44
90	7.73	1.85	0.24	0.08	0.063	0.68	1.67
91	7.73	1.85	0.24	0.08	0.100	0.73	1.62
92	7.73	1.85	0.24	0.08	0.126	0.80	1.87
93	7.73	1.85	0.24	0.08	0.154	0.80	2.03
94	7.73	1.85	0.24	0.08	0.181	0.72	1.99
95	5.23	1.30	0.35	0.11	0.045	0.87	2.23
96	5.23	1.30	0.35	0.11	0.085	0.90	2.05
97	5.23	1.30	0.35	0.11	0.126	0.98	2.25
100	4.05	1.05	0.45	0.14	0.055	0.97	1.81
101	4.05	1.05	0.45	0.14	0.110	0.98	1.71
102	4.05	1.05	0.45	0.14	0.148	1.02	2.14
103	4.05	1.05	0.45	0.14	0.181	1.02	2.19
105	3.20	0.87	0.57	0.18	0.079	1.02	1.65
106	3.20	0.87	0.57	0.18	0.118	1.04	1.95
107	3.20	0.87	0.57	0.18	0.147	1.07	2.13
108	3.20	0.87	0.57	0.18	0.180	1.00	2.20
109	3.20	0.87	0.57	0.18	0.189	1.06	2.25
111	2.44	0.72	0.75	0.24	0.048	0.88	1.29
112	2.44	0.72	0.75	0.24	0.092	0.96	1.36
113	2.44	0.72	0.75	0.24	0.144	1.04	1.41
114	2.44	0.72	0.75	0.24	0.164	1.11	1.45
115	2.44	0.72	0.75	0.24	0.177	1.11	1.50

APPENDIX III

MAXIMUM HORIZONTAL AND VERTICAL WAVE FORCE DATA

Run No. 1 - 28:   Depth = 17.5 inches

Run No.	$\frac{2\pi a}{L}$	$\frac{H}{2a}$	$\frac{F_{H\ max.}}{\gamma a^3}$	$\frac{F_{V\ max.}}{\gamma a^3}$
1	0.13	0.053	0.0164	0.114
2	0.13	0.101	0.0323	0.252
3	0.13	0.157	0.0534	0.378
4	0.13	0.207	0.0685	0.540
5	0.13	0.261	0.0888	0.665
6	0.23	0.075	0.0277	0.159
7	9.23	0.151	0.0620	0.314
8	0.23	0.227	0.0908	0.461
9	0.23	0.304	0.1215	0.611
10	0.23	0.369	0.1440	0.742
11	0.32	0.099	0.0346	0.159
12	0.32	0.190	0.0722	0.279
13	0.32	0.284	0.1078	0.466
14	0.32	0.361	0.1410	0.584
15	0.41	0.107	0.0289	0.107
16	0.41	0.206	0.0576	0.210
17	0.41	0.301	0.0873	0.316
18	0.41	0.368	0.1178	0.382
19	0.50	0.116	0.0244	0.079
20	0.50	0.197	0.0432	0.128
21	0.50	0.262	0.0575	0.168
22	0.50	0.310	0.0713	0.186
23	0.50	0.343	0.0823	0.212
25	0.64	0.015	0.0146	0.033
26	0.64	0.022	0.0220	0.046
27	0.64	0.027	0.0273	0.057
28	0.64	0.031	0.0311	0.067

Run No. 39 - 69: Depth = 14.0 inches

Run No.	$\dfrac{2\pi a}{L}$	$\dfrac{H}{2a}$	$\dfrac{F_H \text{ max.}}{\gamma a^3}$	$\dfrac{F_V \text{ max.}}{\gamma a^3}$
39	0.14	0.075	0.0232	0.202
40	0.14	0.109	0.0370	0.306
41	0.14	0.158	0.0615	0.426
42	0.14	0.186	0.0745	0.552
43	0.14	0.207	0.0850	0.673
44	0.14	0.255	0.1046	0.765
45	0.19	0.055	0.0237	0.142
46	0.19	0.118	0.0519	0.308
47	0.19	0.147	0.0690	0.377
48	0.19	0.223	0.1090	0.593
49	0.19	0.258	0.1290	0.689
50	0.19	0.298	0.1490	0.304
51	0.28	0.067	0.0328	0.136
52	0.28	0.149	0.0760	0.316
53	0.28	0.215	0.1140	0.446
54	0.28	0.283	0.1500	0.511
55	0.28	0.317	0.1742	0.682
56	0.42	0.085	0.0425	0.124
57	0.42	0.185	0.0850	0.259
58	0.42	0.252	0.1210	0.378
59	0.42	0.294	0.1442	0.455
60	0.42	0.347	0.1736	0.548
61	0.51	0.103	0.0371	0.106
62	0.51	0.186	0.0743	0.197
63	0.51	0.244	0.1023	0.271
64	0.51	0.298	0.1311	0.366
65	0.51	0.308	0.1446	0.392
66	0.73	0.101	0.0232	----
67	0.73	0.165	0.0429	0.096
68	0.73	0.214	0.0556	0.127
69	0.73	0.223	0.0603	0.138

Run No. 55A - 69A, 70 - 80:   Depth = 10.5 inches

Run No.	$\dfrac{2\pi a}{L}$	$\dfrac{H}{2a}$	$\dfrac{F_{H\ max.}}{\gamma a^3}$	$\dfrac{F_{V\ max.}}{\gamma a^3}$
55A	0.15	0.048	0.0140	0.157
56A	0.15	0.087	0.0304	0.229
57A	0.15	0.106	0.0454	0.338
61A	0.21	0.056	0.0171	0.146
62A	0.21	0.114	0.0476	0.268
63A	0.21	0.176	0.0800	0.436
64A	0.21	0.207	0.1110	0.582
65A	0.21	0.275	0.1380	0.681
66A	0.30	0.075	0.0453	0.175
67A	0.30	0.146	0.0910	0.346
68A	0.30	0.210	0.1495	0.519
69A	0.30	0.226	0.1685	0.567
70	0.42	0.074	0.0496	0.158
71	0.42	0.156	0.0975	0.314
72	0.42	0.216	0.1300	0.447
73	0.42	0.267	0.1669	0.560
74	0.49	0.087	0.0436	0.143
75	0.49	0.158	0.1046	0.272
76	0.49	0.224	0.1390	0.399
77	0.49	0.267	0.1675	0.475
78	0.75	0.085	0.0417	0.095
79	0.75	0.157	0.0806	0.202
80	0.75	0.218	0.1064	0.264

Run No. 89 - 115:   Depth = 7 inches

Run No.	$\dfrac{2\pi a}{L}$	$\dfrac{H}{2a}$	$\dfrac{F_H \text{ max.}}{\gamma a^3}$	$\dfrac{F_V \text{ max.}}{\gamma a^3}$
89	0.24	0.040	0.0268	0.058
90	0.24	0.063	0.0428	0.105
91	0.24	0.100	0.0700	0.162
92	0.24	0.126	0.1010	0.236
93	0.24	0.154	0.1230	0.312
94	0.24	0.181	0.1300	0.360
95	0.35	0.045	0.0390	0.100
96	0.35	0.085	0.0765	0.174
97	0.35	0.126	0.1239	0.284
100	0.45	0.055	0.0535	0.099
101	0.45	0.110	0.1080	0.188
102	0.45	0.148	0.1510	0.316
103	0.45	0.181	0.1850	0.396
105	0.57	0.079	0.0805	0.131
106	0.57	0.118	0.1228	0.230
107	0.57	0.147	0.1570	0.313
108	0.57	0.180	0.1800	0.396
109	0.57	0.189	0.2000	0.425
111	0.75	0.048	0.0422	0.062
112	0.75	0.092	0.0882	0.125
113	0.75	0.144	0.1495	0.203
114	0.75	0.164	0.1820	0.237
115	0.75	0.177	0.1963	0.267

APPENDIX IV

LINEAR FORCE COEFFICIENT CHARTS

The following maximum horizontal and vertical force charts are presented to show the linear variation of force to wave height. Also, the linear slopes of these charts were used to determine the maximum experimental horizontal and vertical force coefficients (See Appendix V) which were compared to corresponding theoretical points as shown by Figures (14-21).
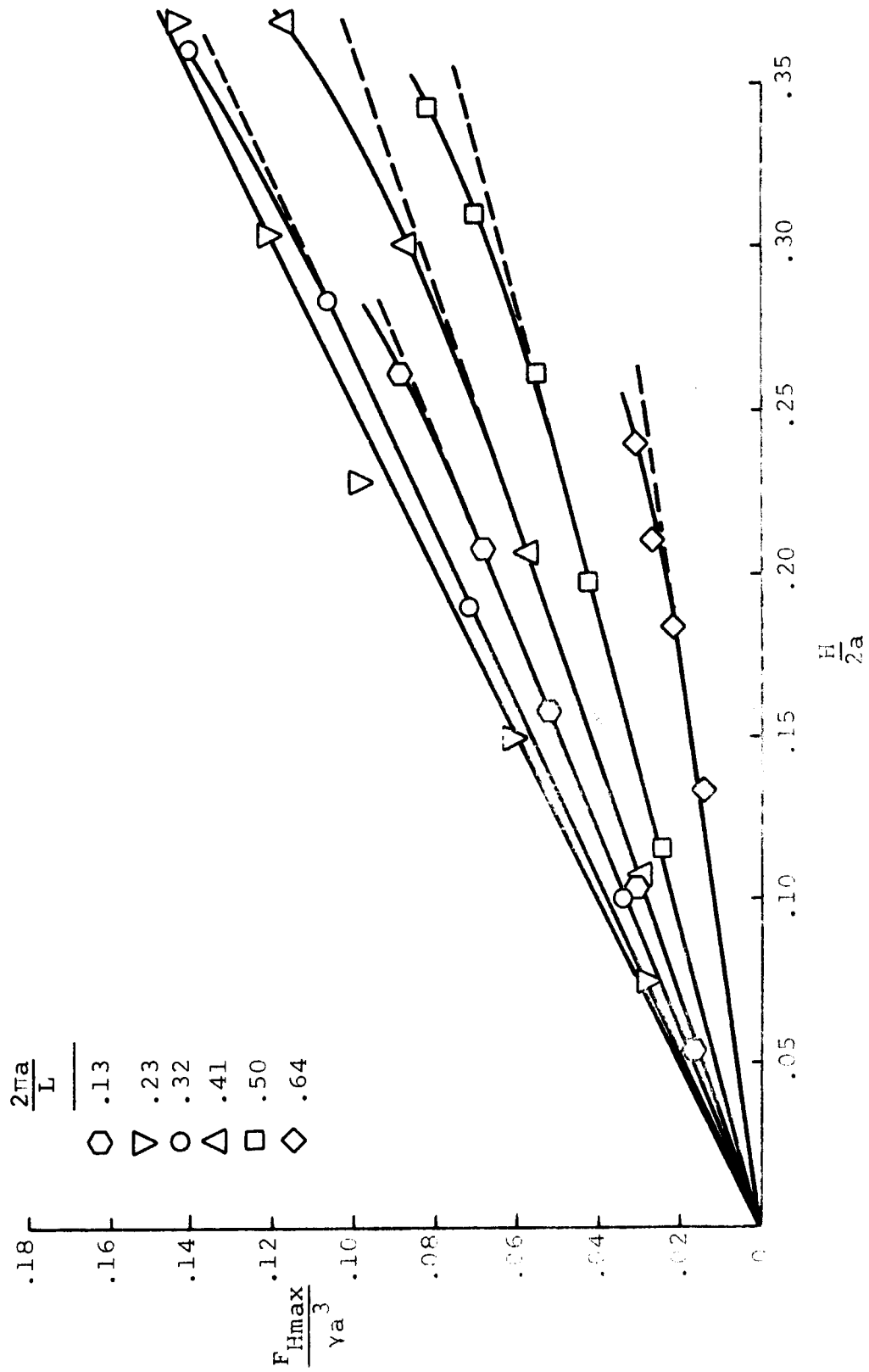
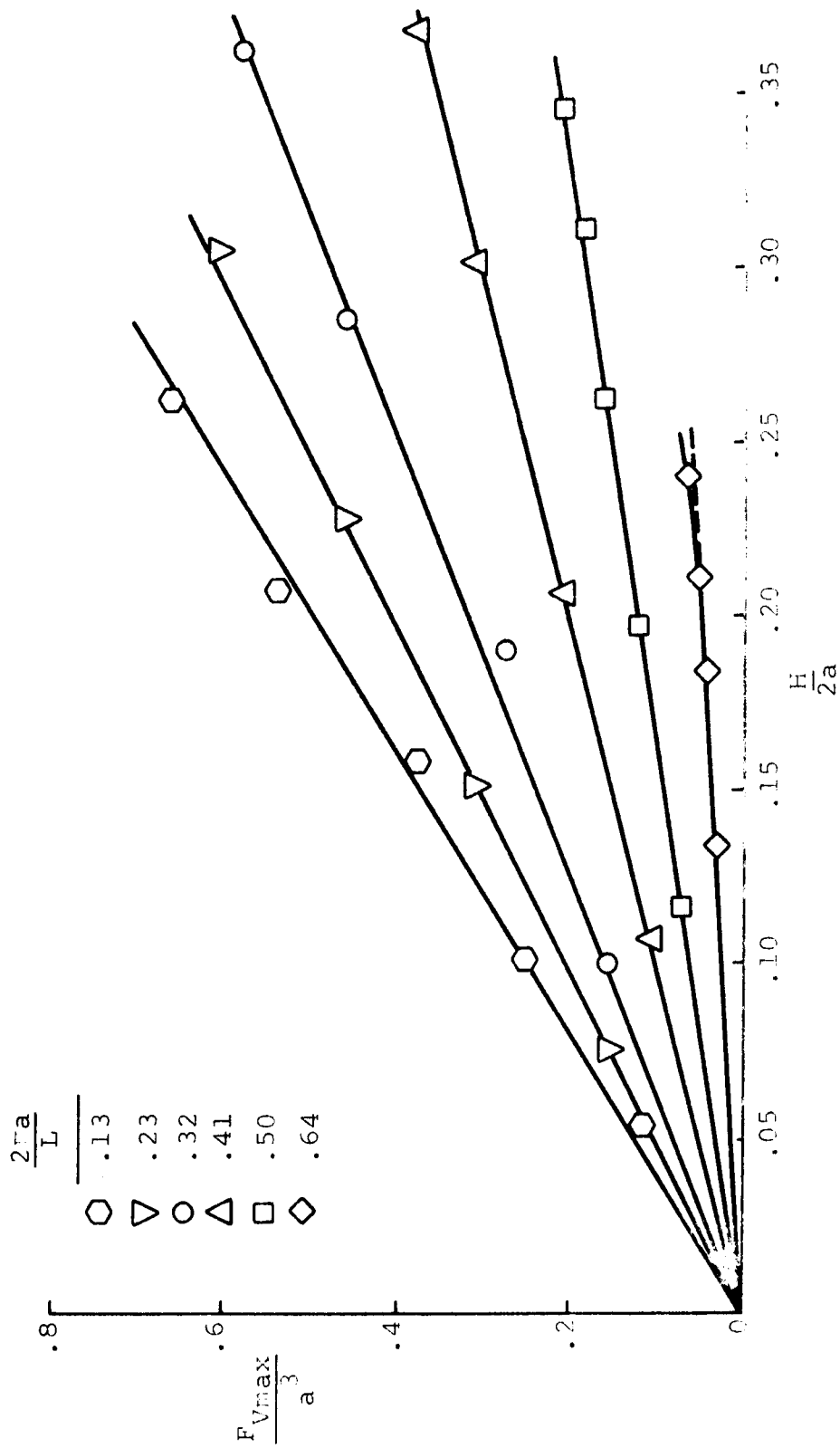Figure 22. Maximum horizontal force for $\frac{h}{a} = 5$.

Legend:

$\frac{2\pi a}{L}$	
⬡	.13
▽	.23
○	.32
◁	.41
☐	.50
◇	.64

Vertical axis: $\frac{F_{Hmax}}{\gamma a^3}$

Horizontal axis: $\frac{H}{2a}$

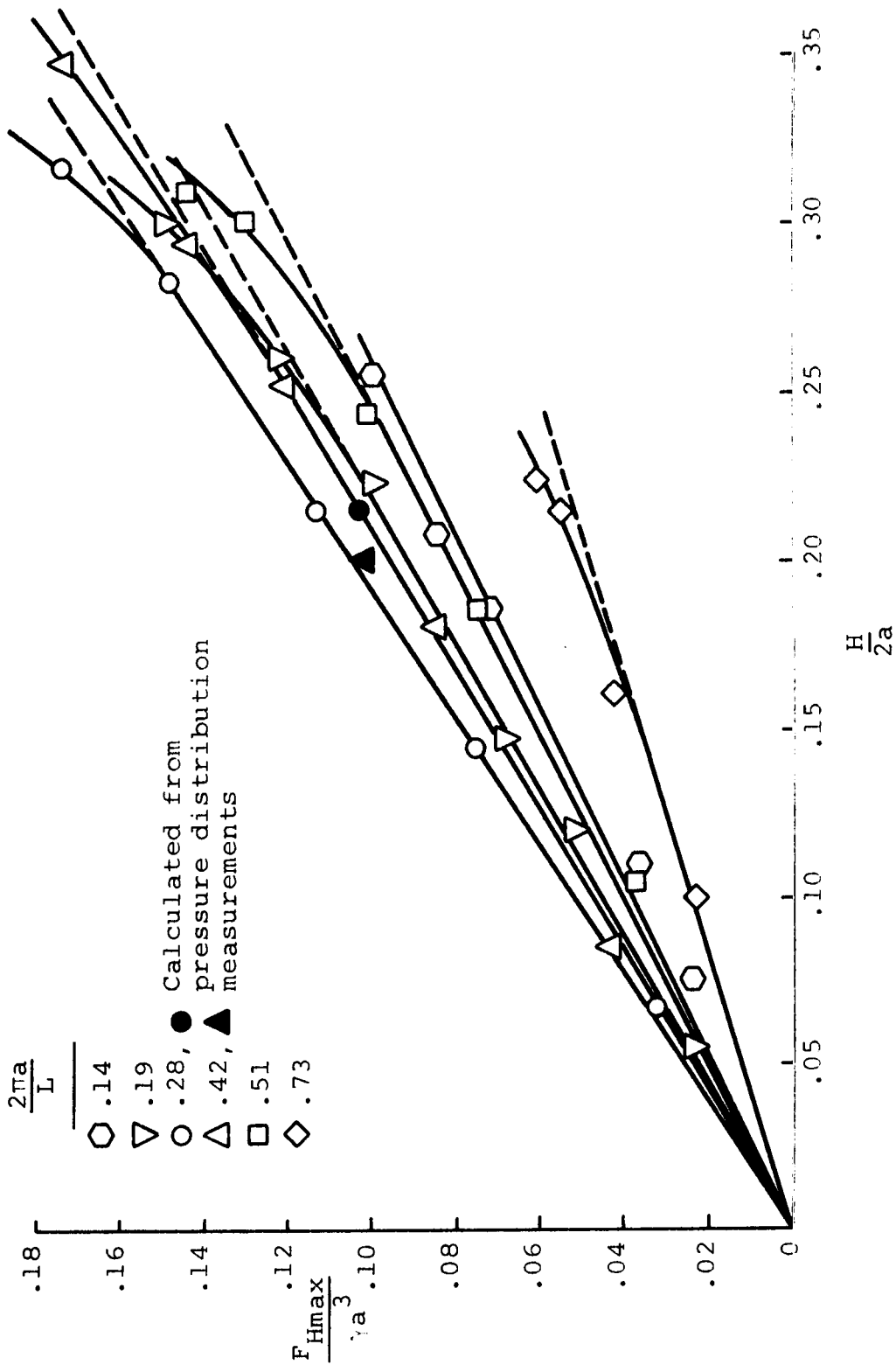Figure 23. Maximum vertical force for $\frac{h}{a} = 5$.

74

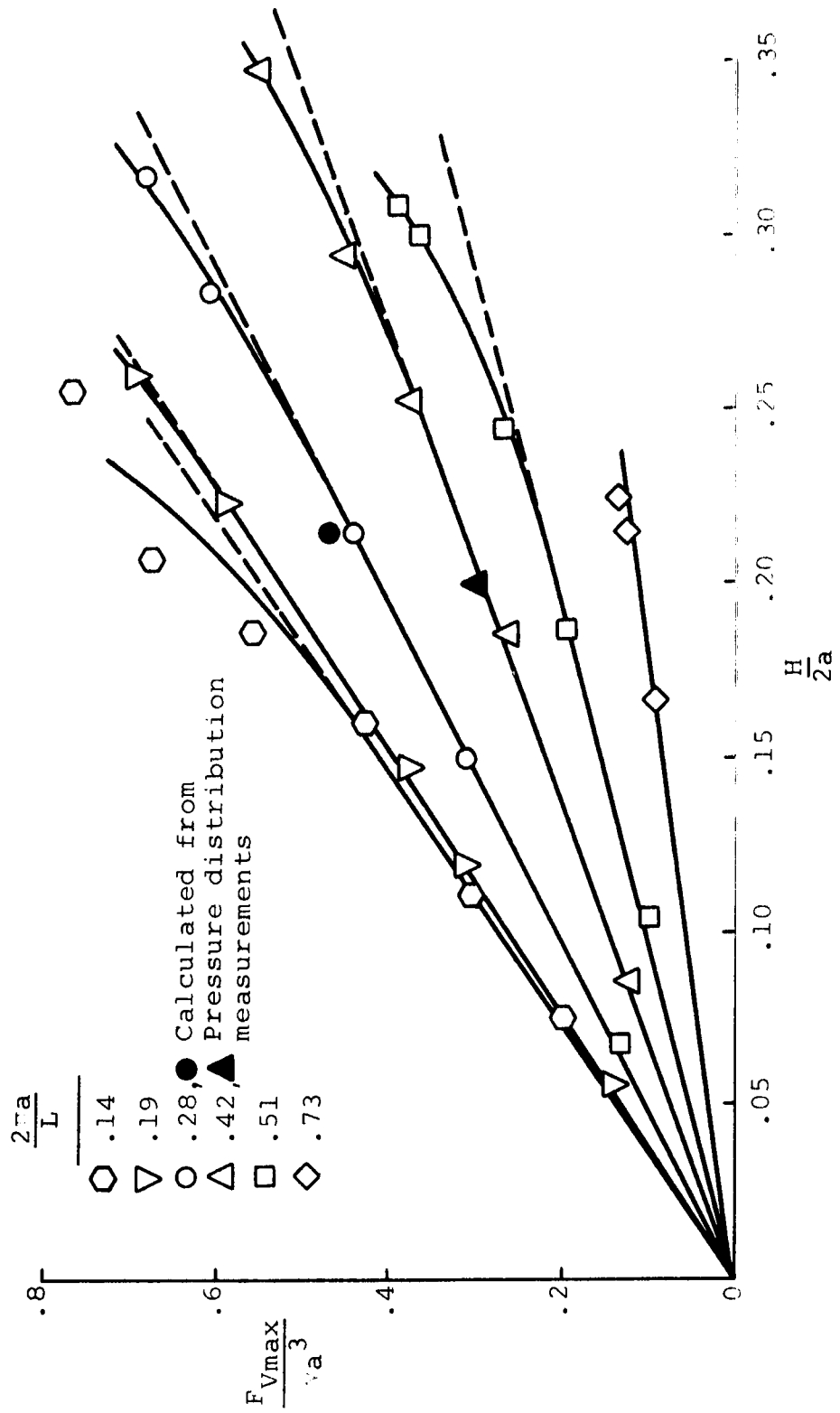Figure 24. Maximum horizontal force for $\frac{h}{a} = 4$.

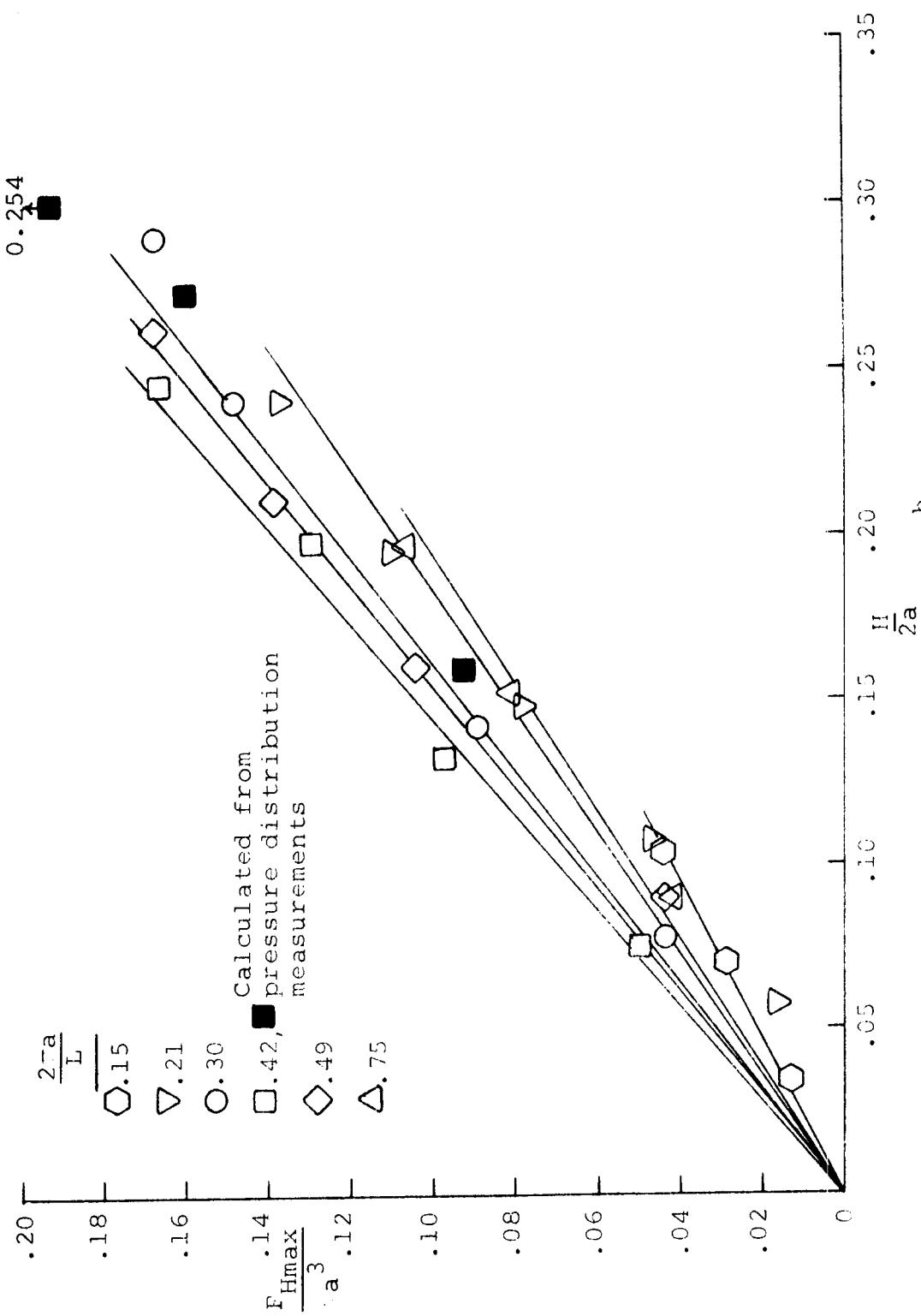Figure 25. Maximum vertical force for $\frac{h}{a} = 4$.

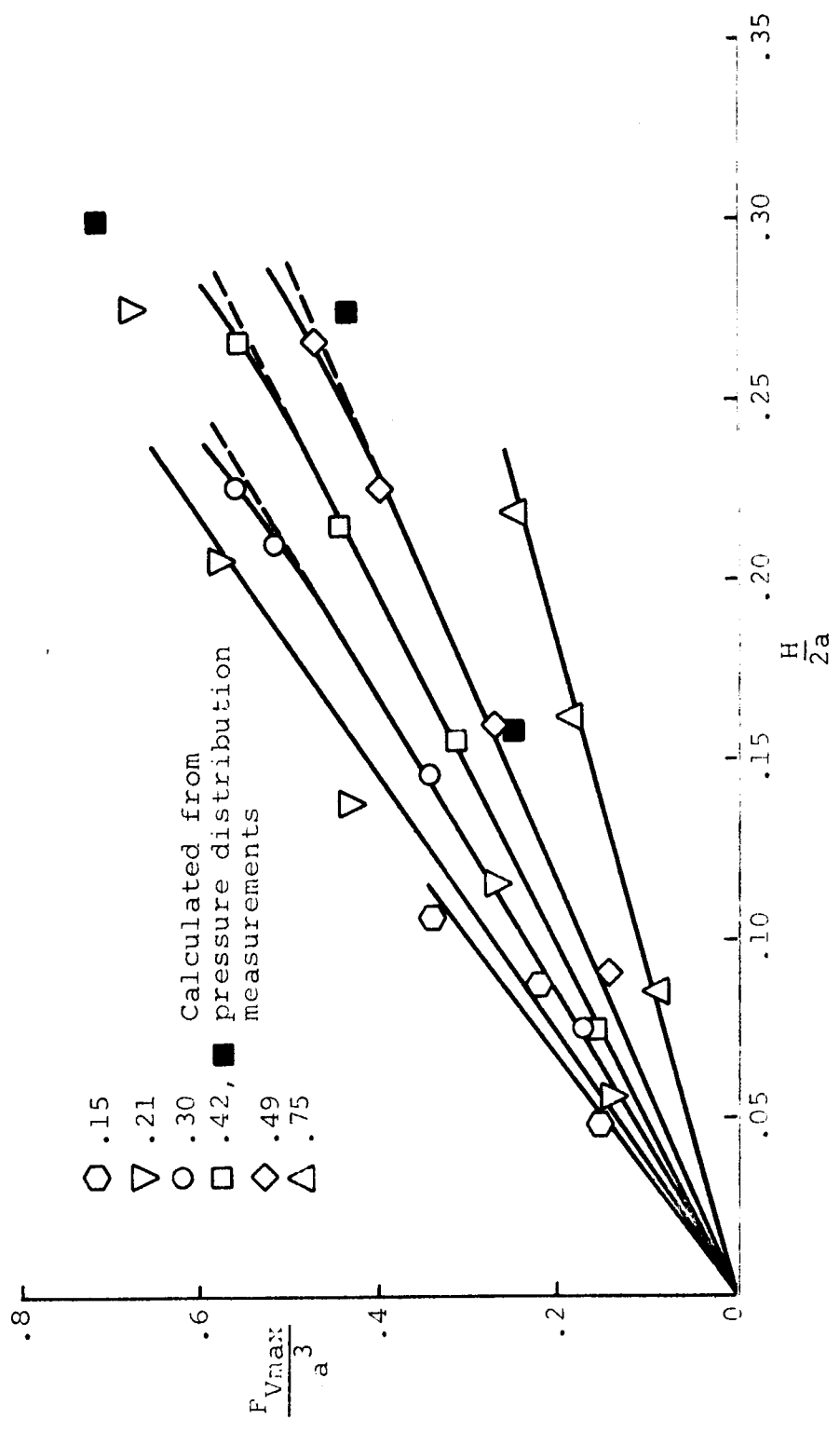Figure 26. Maximum horizontal force for $\frac{h}{a} = 3$.

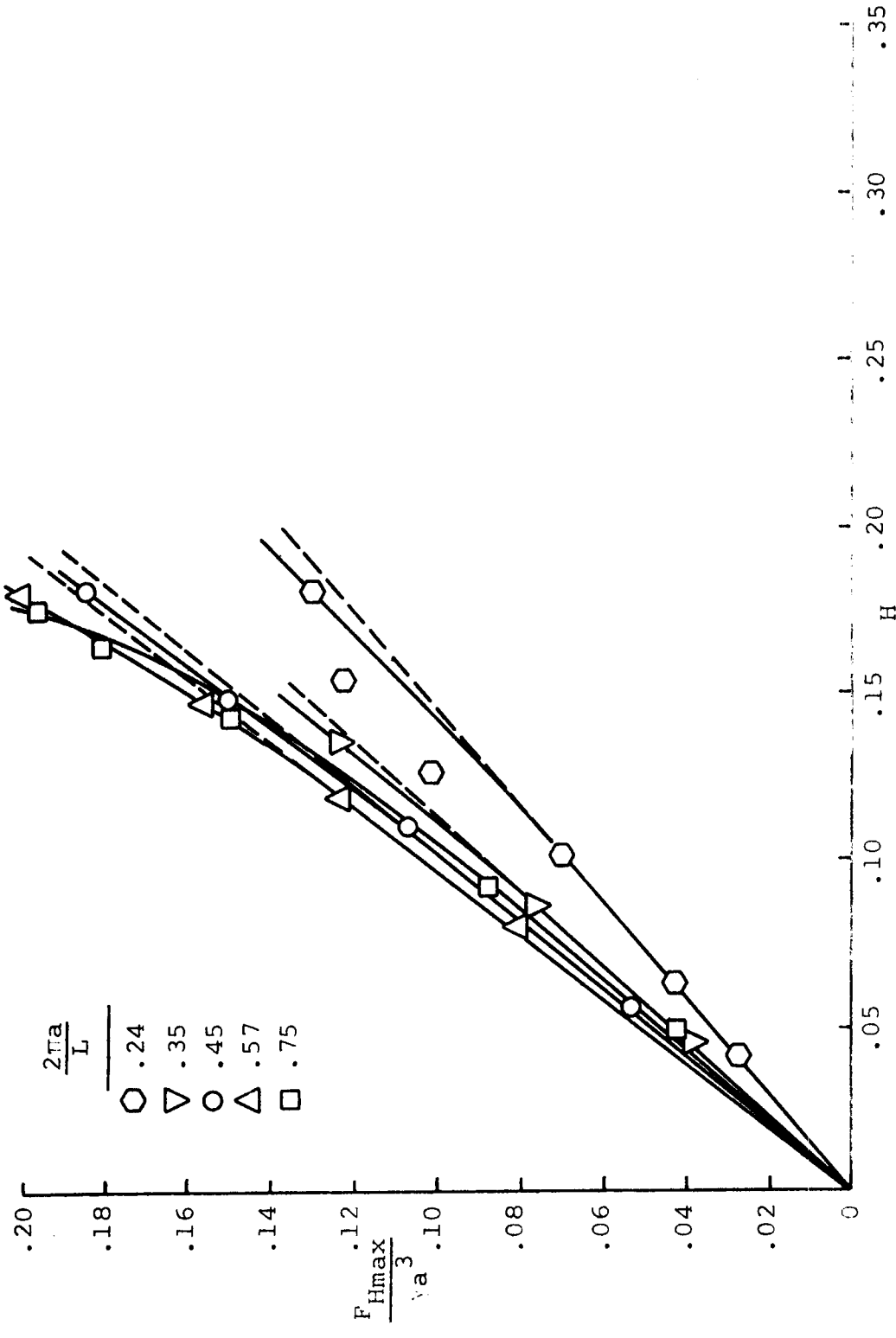Figure 27. Maximum vertical force for $\frac{h}{a} = 3$.

Figure 28. Maximum horizontal force for $\frac{h}{a} = 2$.
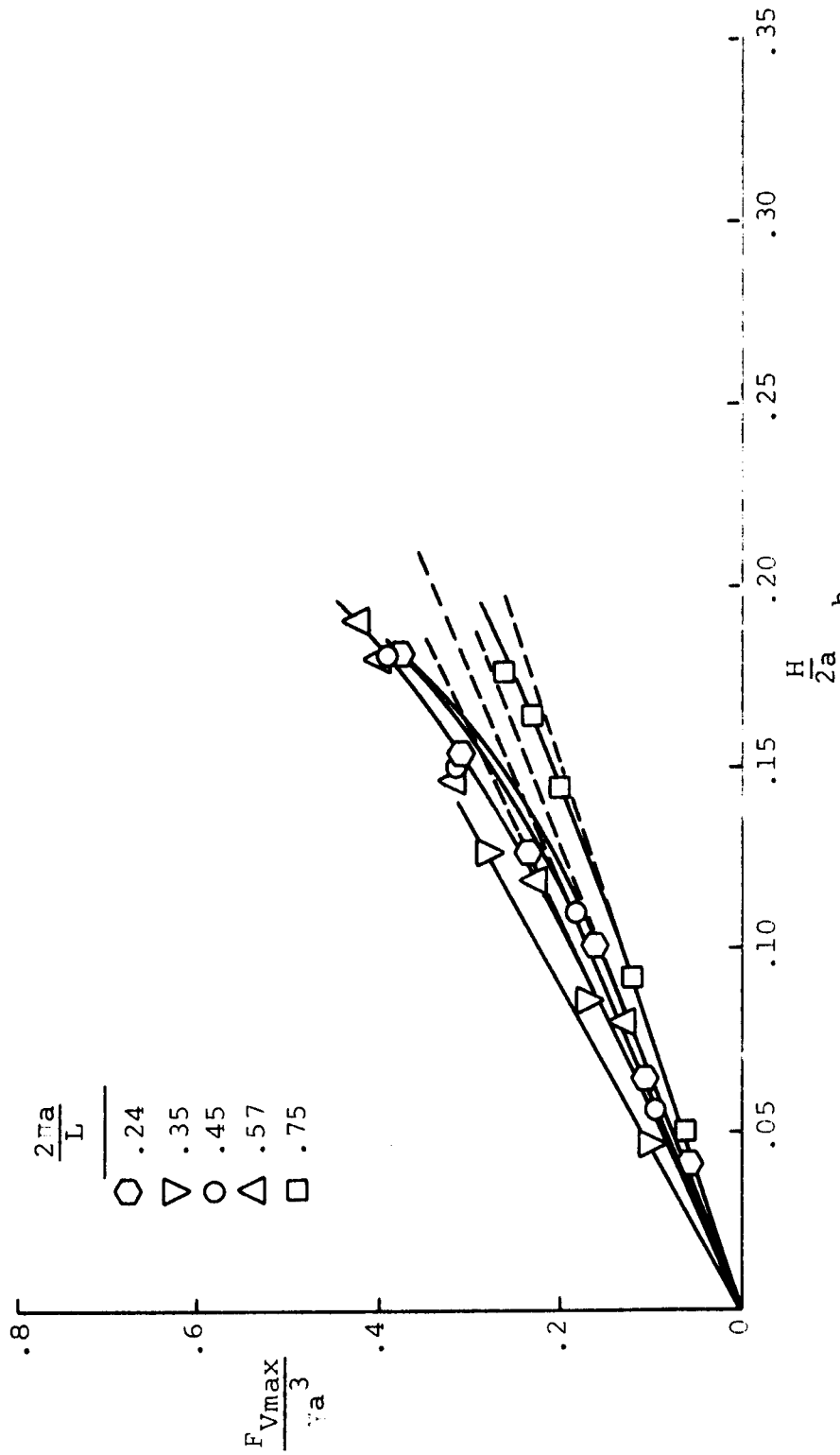
Figure 29. Maximum vertical force for $\frac{h}{a} = 2$.

APPENDIX V

EXPERIMENTAL LINEAR HORIZONTAL AND VERTICAL

FORCE COEFFICIENTS

Run No. 1 - 28:   Depth = 17.5 inches

$\frac{2\pi a}{L}$	f_x	f_y
0.13	0.332	2.50
0.23	0.400	2.05
0.32	0.376	1.60
0.41	0.278	1.03
0.50	0.213	0.63
0.64	0.120	0.27

Run No. 39 - 69:   Depth = 14.0 inches

0.14	0.374	2.76
0.19	0.460	2.62
0.28	0.525	2.08
0.42	0.475	1.48
0.51	0.408	1.07
0.73	0.236	0.58

Run No. 55A - 69A, 70 - 80:   Depth = 10.5 inches

0.15	0.433	3.02
0.21	0.550	2.74
0.30	0.630	2.42
0.42	0.695	2.04
0.49	0.652	1.74
0.75	0.520	1.10

Run No. 89 - 115:   Depth = 7.0 inches

$\dfrac{2\pi a}{L}$	f_x	f_y
0.24	0.670	1.62
0.35	0.895	2.20
0.45	1.020	1.90
0.57	1.035	1.76
0.75	0.960	1.38

APPENDIX VI

LIST OF SYMBOLS

Symbol	Quantity	Units	Dimension
A	Wave amplitude	ft	L
a	Radius of hemisphere	ft	L
C_m	Induced mass coefficient	-	-
F_B	Buoyant force	lb	F
F_I	Inertial force	lb	F
F	Total horizontal force	lb	F
F_{Hmax}	Maximum horizontal force	lb	F
f_x	Horizontal force coefficient	-	-
F_V	Vertical force	lb	F
F_{Vmax}	Maximum vertical force	lb	F
f_y	Vertical force coefficient	-	-
F_R	Force reading	lb	F
F_p	Internal pressure force reading	lb	F
g	Acceleration of gravity	ft/sec^2	L/T^2
h	Total depth	ft	L
H	Wave height	ft	L
k	Wave number $(2\pi/L)$	1/ft	$1/L$
L	Wave length	ft	L
L_o	Deep water wave length	ft	L
P	Subsurface pressure	lb/ft^2	F/L^2
P_o	Amplitude of pressure	lb/ft^2	F/L^2

t	Time or duration	sec	T
T	Wave period	sec	T
u	Velocity in X-direction	ft/sec	L/T
$\dot{u}$	Local acceleration	ft/sec^2	L/T^2
$\forall$	Volume	ft^3	L^3
X	Horizontal distance, in direction of wave propagation	ft	L
Z	Vertical distance, with origin in surface	ft	L
π	3.1416	–	–
ρ	Mass density	$lb\text{-}sec^2/ft^4$	$F\text{-}T^2/L^4$
γ	Specific weight	lb/ft^3	F/L^3
σ	Wave angular frequency = alternate to $\omega = 2\pi/T$	1/sec	1/T
φ	Velocity potential	ft^2/sec	L^2/T
θ	Angular displacement	radians	–
δ	Phase shift reading	radians	–
β	Angular displacement in the vertical plane	radians	–
α	Angular displacement in the horizontal plane	radians	–
λ	Phase shift angle	radians	–